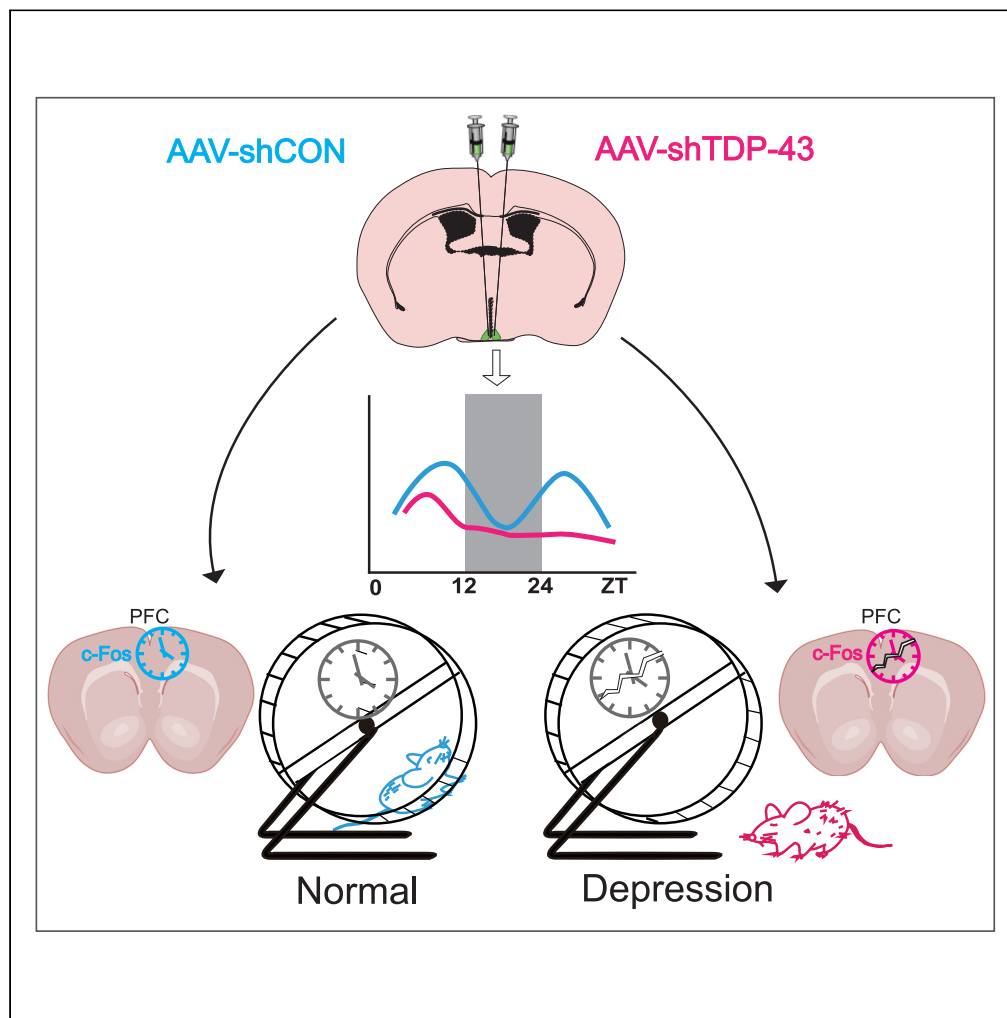


Article

TDP-43 deficiency in suprachiasmatic nucleus perturbs rhythmicity of neuroactivity in prefrontal cortex



Hongxia Zhang,
Chen Chen, Eric
Erquan Zhang,
Xiaotian Huang

zhangerquan@mibs.ac.cn
(E.E.Z.)
xthuang@ncu.edu.cn (X.H.)

Highlights

Loss of TDP-43
dysregulates the
intracellular clockwork

Knockdown of TDP-43 in
SCN induces locomotor
arrhythmia

TDP-43 deficiency in SCN
disrupts c-Fos rhythm in
PFC

TDP-43 knockdown in SCN
leads to behavioral
abnormality

Zhang et al., iScience 27,
109522
April 19, 2024 © 2024 The
Authors. Published by Elsevier
Inc.
[https://doi.org/10.1016/
j.isci.2024.109522](https://doi.org/10.1016/j.isci.2024.109522)

Article

TDP-43 deficiency in suprachiasmatic nucleus perturbs rhythmicity of neuroactivity in prefrontal cortex

Hongxia Zhang,^{1,2} Chen Chen,² Eric Erquan Zhang,^{2,3,*} and Xiaotian Huang^{1,*}

SUMMARY

Individuals within the amyotrophic lateral sclerosis and frontotemporal dementia disease spectrum (ALS/FTD) often experience disruptive mental behaviors and sleep-wake disturbances. The hallmark of ALS/FTD is the pathological involvement of TAR DNA-binding protein 43 (TDP-43). Understanding the role of TDP-43 in the circadian clock holds promise for addressing these behavioral abnormalities. In this study, we unveil TDP-43 as a pivotal regulator of the circadian clock. TDP-43 knockdown induces intracellular arrhythmicity, disrupts transcriptional activation regulation, and diminishes clock genes expression. Moreover, our experiments in adult mouse reveal that TDP-43 knockdown, specifically within the suprachiasmatic nucleus (SCN), induces locomotor arrhythmia, arrhythmic c-Fos expression, and depression-like behavior. This observation offers valuable insights into the substantial impact of TDP-43 on the behavioral aberrations associated with ALS/FTD. In summary, our study illuminates the significance of TDP-43 in circadian regulation, shedding light on the circadian regulatory mechanisms that may elucidate the pathological underpinnings of ALS/FTD.

INTRODUCTION

The circadian clock is an intrinsic timekeeping system intricately linked to human health, governing vital processes such as the sleep-wake cycle, emotional regulation, neurotransmitter and hormone secretion, and various other biological functions.^{1,2} In mammals, the circadian clockwork comprises a network of clock genes and their protein products, orchestrating a near-24-h cycle through a transcription-translation negative feedback loop. Central components of this clockwork include the bHLH-PAS transcription factor circadian locomotor output cycles kaput (CLOCK) and brain and muscle ARNT-like 1 (BMAL1) and their specific repressors period (PER) and cryptochrome (CRY).³ The CLOCK/BMAL1 heterodimer binds to the E-box regions of *PER* and *CRY* gene promoters, initiating the transcription and protein synthesis of PERs and CRYs. Subsequently, PER and CRY form heterodimers, acting as transcriptional repressors to dampen the activation of CLOCK/BMAL1.⁴⁻⁶

Disruptions in the circadian clock have been associated with a spectrum of diseases, with recent research emphasizing alterations in circadian rhythms in patients with neurodegenerative conditions and related animal models.⁷

One prominent player in neurodegenerative diseases is TAR DNA binding protein 43 (TDP-43), a conserved RNA-binding protein with pivotal roles in RNA splicing, stability, trafficking, and microRNA regulation.⁸ Importantly, both amyotrophic lateral sclerosis (ALS) and frontotemporal dementia (FTD) are characterized by TDP-43 pathology, with cytoplasmic mis-localization and aggregation of TDP-43 being common features in affected individuals.⁹ While previous investigations have primarily focused on the impact of TDP-43 mutations in hereditary ALS/FTD and its critical role in neuropathy, recent studies have unveiled that both an increase and decrease in TDP-43 levels can result in neuronal loss.^{10,11}

Furthermore, patients with FTD often show distinct patterns of destruction in the suprachiasmatic nucleus (SCN). This destruction leads to an alteration of endogenous circadian rhythm, exhibiting disruptions in their rest-activity and sleep-wake patterns, including increased nocturnal activity and reduced morning activity, suggesting a potential phase delay.¹²⁻¹⁴ Elevated evening cortisol levels have been observed in ALS patients compared to healthy individuals.¹⁵ Some studies have even suggested that circadian rhythm dysfunction may accelerate ALS onset and progression in mouse models.¹⁶ Notably, there are significant connections between mood disorders and ALS/FTD, with overlapping symptoms and neuropathology. Mood stabilizers like lithium have demonstrated efficacy in improving symptoms in ALS/FTD patients.^{17,18} Nevertheless, few studies have explored the possibility that TDP-43 may exacerbate neurodegeneration through disruption of circadian clock regulation.

¹Department of Medical Microbiology, Jiangxi Medical College, Nanchang University, Nanchang 330006, China

²National Institute of Biological Sciences, Beijing 102206, China

³Lead contact

*Correspondence: zhangerquan@nibs.ac.cn (E.E.Z.), xthuang@ncu.edu.cn (X.H.)
<https://doi.org/10.1016/j.isci.2024.109522>



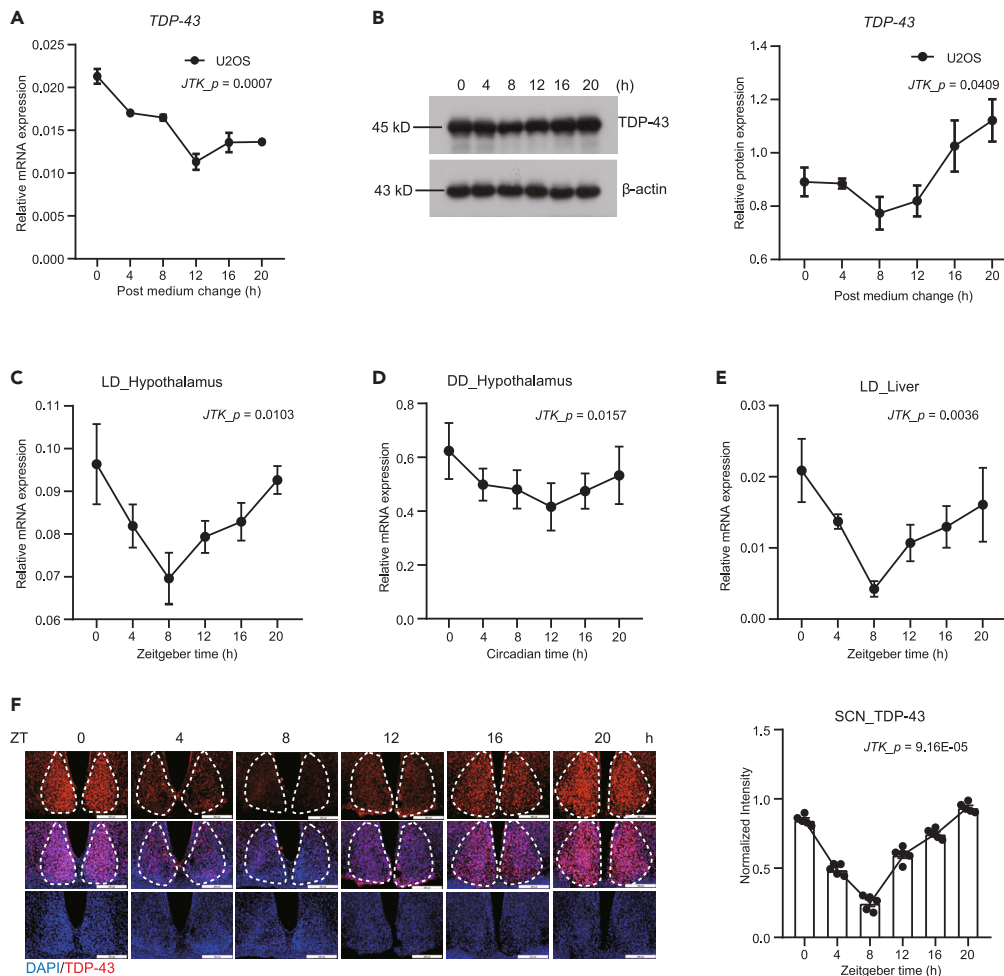


Figure 1. Rhythmic oscillations of TDP-43 in vitro and in vivo

(A) Temporal qPCR analysis illustrating robust rhythmic expression patterns of *TDP-43* in U2OS cells. $n = 3$ samples for each time point. JTK_Cycle analysis confirms the significance of this rhythmicity ($p = 0.000686$).

(B) Western blot analysis revealing rhythmic protein levels of TDP-43 in U2OS cells. $n = 3$ samples for each time point. JTK_Cycle analysis confirms the significance of rhythmicity ($p = 0.0409$).

(C–E) Time course qPCR demonstrating rhythmic expression of *Tdp-43* in the hypothalamus in LD and DD conditions and liver. $n = 4$ male mice for each time point. JTK_Cycle analysis was conducted to evaluate the rhythmicity of *Tdp-43* expression.

(F) Temporal immunostaining of TDP-43 in the SCN region of male mice, with quantification of expression. The dotted line indicates the SCN. JTK_Cycle analysis confirms significant rhythmicity ($p = 9.16E-05$). Immunostained slices (40 μm thickness per slice) were labeled with DAPI (blue) and TDP-43 antibody (red). 4–6 SCN regions per mouse and $n = 5$ mice for each time point. Scale bar, 200 μm . $JTK_p < 0.05$ indicates significantly rhythmic. Data are presented as mean \pm SEM.

In our earlier investigation, we identified a super-complex by subjecting rhythmic *Bmal1*^{-/-} fibroblasts to tandem affinity purification. Within this complex, we detected several putative clock regulatory proteins, including TDP-43 (data file S1), suggesting a potential interaction between TDP-43 and clock genes, hinting at a role for TDP-43 in modulating the circadian clockwork.¹⁹

To elucidate the involvement of TDP-43 in circadian clock regulation and its broader implications for ALS/FTD, we conducted a series of experiments involving TDP-43 knockdown in cellular models to investigate its influence on circadian rhythms and clock gene expressions. Additionally, we employed *Tdp-43* knockdown in mouse models to explore changes in behavioral aspects associated with ALS/FTD.

RESULTS

TDP-43 exhibits robust circadian rhythmicity

Given our previous findings suggesting that TDP-43 may potentially regulate circadian amplitude, period, or phase,¹⁹ and a study demonstrating TDP-43 could enhance CRY1 and CRY2 protein stabilities and levels,²⁰ we aimed to determine if TDP-43 behaves as a clock-associated gene, contributing to the regulation of circadian rhythms in mammals. From the analysis of time course qPCR, we observed robust rhythmic mRNA expression of *TDP-43* in U2OS cells (Figure 1A). Concurrently, we assessed the rhythmicity of TDP-43 protein level, which yielded

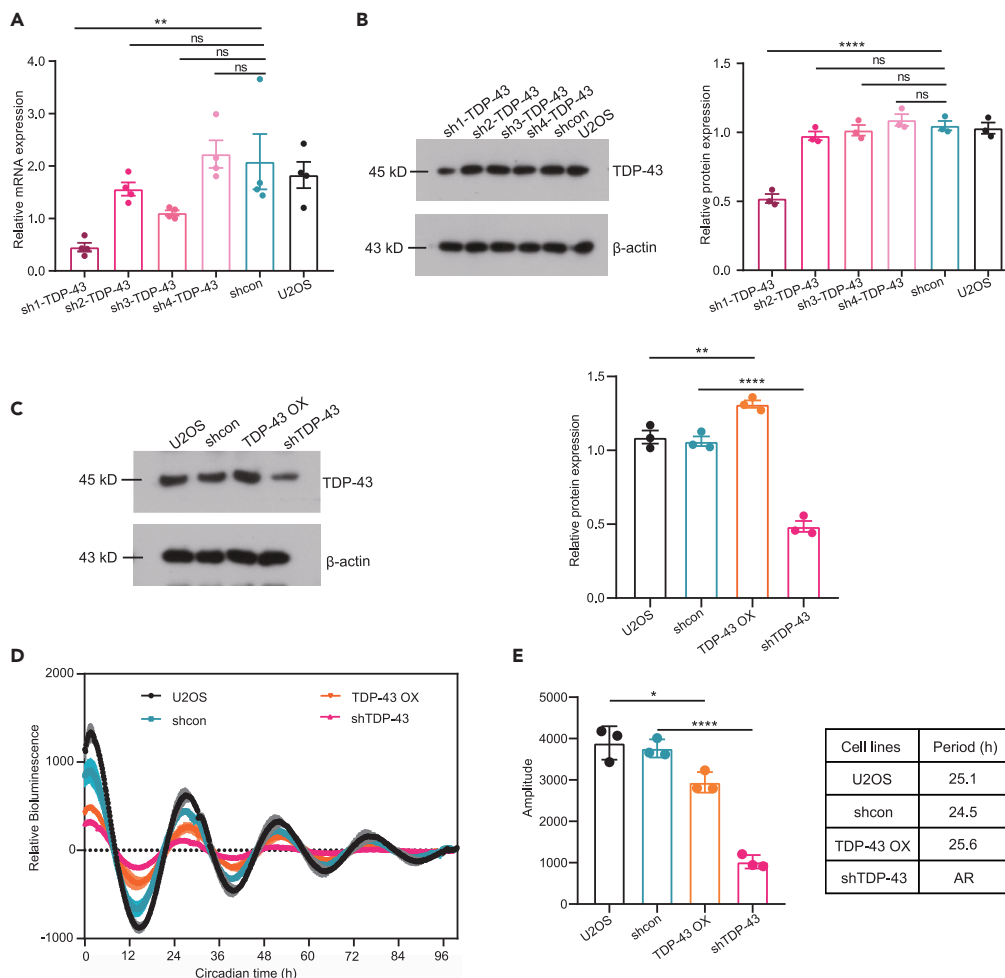


Figure 2. TDP-43 knockdown causes intracellular arrhythmicity

(A) qPCR data depicting the knockdown efficiency of shRNAs targeting *TDP-43* in U2OS cells. $n = 4$ represents technical replicates. (B) Western blot results presenting the knockdown efficiency of shRNAs targeting *TDP-43* in U2OS cells, with quantification of *TDP-43* levels. $n = 3$ samples for each group. (C) Western blot results presenting the protein levels of *TDP-43* in U2OS, shCON, shTDP-43, and TDP-43 OX (overexpressed *TDP-43*) cells, with their quantification. $n = 3$ samples per group. (D) Representative *PER2-LUC* rhythms in WT, shTDP-43, shCON, and TDP-43 OX cells. $n = 3$ samples per group. (E) Quantitative amplitude and period analysis of WT, shTDP-43, shCON, and TDP-43 OX cells detected in (D). One-way ANOVA with multiple comparison test for (A)–(C) and (E); Quantifications are presented as mean \pm SEM, ns indicates no significance; * $p < 0.05$, ** $p < 0.01$, *** $p < 0.001$, **** $p < 0.0001$.

the result consistent with the qPCR data (Figure 1B). Next, we extended our analysis to the hypothalamus and liver to explore whether *Tdp-43* follows a circadian pattern in these tissues. Time course qPCR again revealed clear circadian oscillations in *Tdp-43* expression, with SCN peaking at Zeitgeber time (ZT) 20 under light-dark conditions (LD 12:12 h) and CT0 in constant darkness (DD) entrainment (Figures 1C and 1D), with liver peaking at ZT0 in LD phase (Figure 1E). Furthermore, immunofluorescence staining using a *TDP-43* antibody in the SCN showed a distinct circadian rhythm in *TDP-43* expression, peaking at ZT 20 (Figure 1F). Collectively, these results strongly support the notion that *TDP-43* exhibits robust rhythmic oscillations in its expression, suggesting *TDP-43* is a clock controlled gene (CCG) in circadian regulation. Consequently, we hypothesized whether *TDP-43* can in turn affect the circadian clockwork.

Loss of *TDP-43* disrupts intracellular rhythmicity

To investigate the role of *TDP-43* in circadian rhythmicity, we initially focused on the impact of *TDP-43* deficiency using short hairpin RNA (shRNA) in U2OS cells. Among four candidate shRNAs targeting *TDP-43*, shRNA1-*TDP-43* exhibited the highest knockdown efficiency, approximately 51.5–77.5% compared to control shRNA (shcon) (Figures 2A and 2B). We then examined whether overexpression or silencing of *TDP-43* in U2OS cells affects circadian rhythmicity. Protein levels of *TDP-43* knockdown and overexpression are depicted in Figure 2C. Cells

with TDP-43 knockdown exhibited a lower amplitude and eventually became arrhythmic, which is consistent with findings of our previous genome-wide RNAi screen, as well as those in a public database (<http://biogps.gnf.org/circadian/>).²¹ Conversely, cells overexpressing TDP-43 did not exhibit significant changes in cellular period but displayed a slightly weaker amplitude (Figures 2D and 2E). These results highlight the critical role of TDP-43 in regulating circadian rhythmicity.

Knockdown of TDP-43 affects intracellular clockwork

To gain further insights into the role of TDP-43 in the circadian clock and its mechanism in perturbing intracellular rhythmicity, we used an E-box promoter-luciferase fusion reporter (E-box-Luc) to investigate the role of TDP-43 in the transcriptional regulation by the core circadian clock proteins, CLOCK-BMAL1. The results showed that CLOCK-BMAL1 binding-dependent transcription of the E-box-Luc increased in the presence of TDP-43 in a gene dosage dependent manner. By contrast, CRY1 expression could suppress CLOCK-BMAL1 activation of luciferase expression (Figure 3A). We then examined whether suppressing with shTDP-43 negatively affected transcriptional activation by CLOCK-BMAL1. We found that TDP-43 knockdown indeed led to reduced CLOCK-BMAL1 activation of luciferase expression, suggesting that deficiency for TDP-43 resulted in inhibition of CLOCK-BMAL1 binding-dependent activation of the E-box promoters (Figure 3B).

Besides that, we collected RNA samples at indicated circadian time points from shTDP-43, shcon, and U2OS cells. The mRNA levels of *CLOCK*, *BMAL1*, *PER2*, and *TDP-43* in shTDP-43 cells were consistently lower than those in shcon and U2OS cells at all time points (Figure 3C). Studies have shown that mature transcript levels of many genes are significantly altered upon TDP-43 depletion, possibly through transcription, splicing, or other post-transcriptional processes.²² To determine whether shTDP-43 downregulates *CLOCK* and *BMAL1* expressions through direct modulation of transcription of pre-RNA or through splicing, we designed three different pairs of pre-RNA primers targeting the intron regions of *CLOCK* and *BMAL1*. The qPCR analysis showed no significant differences in *CLOCK* and *BMAL1* pre-RNA levels among U2OS, shcon, and shTDP-43 groups (Figures S1A and S1B), suggesting that TDP-43 might influence *CLOCK* and *BMAL1* expressions through its post-transcriptional regulation. These findings suggest that the knockdown of TDP-43 disrupts the circadian negative feedback loop and potentially disturbs the rhythmicity of clock genes.

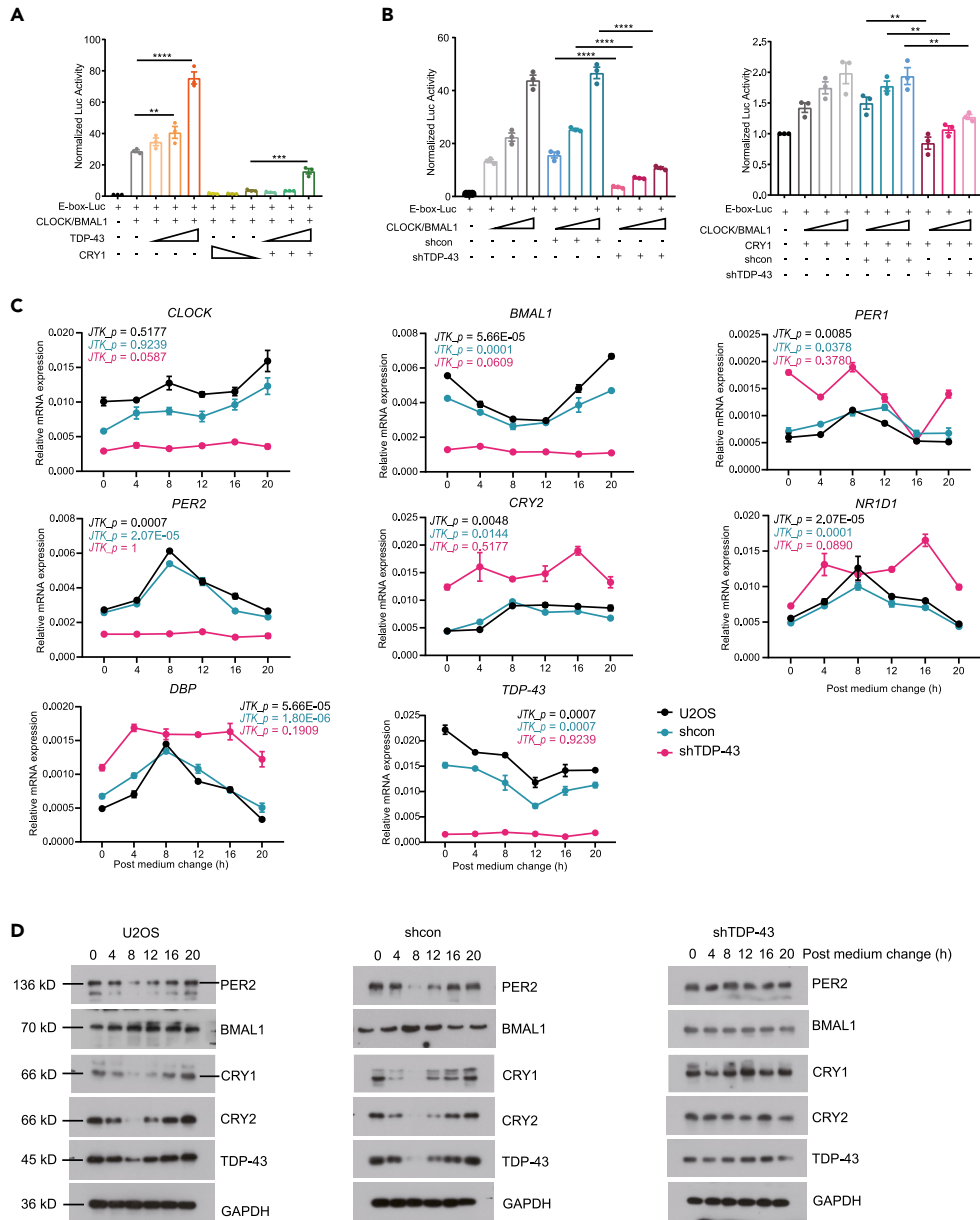
As shown in Figure 3C, the knockdown of TDP-43 resulted in significant reductions in the amplitudes of *CLOCK*, *BMAL1*, and *PER2*. Notably, core clock genes such as *BMAL1*, *PER1*, *PER2*, *CRY2*, *NR1D1*, and *DBP* displayed nearly complete arrhythmicity in shTDP-43 cells, while they exhibited robust rhythmic patterns in shcon and U2OS cells (Figure 3C). Western blot analysis further revealed that the rhythmic expressions of *BMAL1*, *PER2*, *CRY1*, *CRY2*, and *TDP-43* proteins were disrupted by knockdown of TDP-43, whereas these proteins displayed robust rhythmicities in shcon and U2OS cells (Figure 3D; Figure S2). These findings highlight the intricate role of TDP-43 in the circadian clock and its ability to modulate circadian gene expression patterns, shedding light on the mechanisms underlying circadian disruption.

Knockdown of TDP-43 in SCN disrupts circadian rhythm in mice

After establishing that TDP-43 knockdown can induce arrhythmicity in U2OS cells and disrupt the rhythmic expressions of core clock genes, we investigated the effects of shTDP-43 on animals. Specifically, we injected adeno-associated viruses (AAV) encoding shTDP-43 or shCON into the bilateral SCN of C57BL/6J mice (Figure 4A). Following three weeks of virus expression, we conducted western blot and immunofluorescence staining analysis to assess the protein level of TDP-43 in the hypothalamus and SCN, respectively. AAV-shTDP-43 led to a significant decrease in the protein level of TDP-43 compared with AAV-shCON (Figure 4B). This reduction in TDP-43 protein was further confirmed through immunofluorescence staining, where the fluorescence signal of TDP-43 was markedly diminished in the SCN of AAV-shTDP-43 mice (Figure 4C).

Having established the effective knockdown of TDP-43 in the SCN, we next conducted locomotor activity assays to estimate the circadian behaviors in these mice. AAV-shTDP-43 and AAV-shCON mice were entrained under LD cycle for two weeks, followed by further recording under DD phase for two weeks. Interestingly, while the periods of locomotor rhythms in AAV-shTDP-43 and AAV-shCON mice did not significantly differ in LD environment (averaging around 24 and 23.93 h, respectively), AAV-TDP-43 mice displayed a complete loss of circadian rhythmicity when placed in DD phase (Figures 4D and 4E). Moreover, we employed a telemetric transmitter system to record rhythmicity of core body temperature and gross motor activity in both male and female mice. It is worth noting that, in AAV-shTDP-43 mice, obvious rhythmicity similar to that observed in wheel running assays was detected in core body temperatures under LD cycle (period of 21–27 h) and arrhythmicity under DD phase. In contrast, we observed significantly robust clock-driven physiology in core body temperature of AAV-shCON mice under both LD and DD conditions (period of 21–27 h) (Figures 4F and 4G). Furthermore, using the BD2eJTK feature of the web-based Biodare2 toolkit,²³ we found that the amplitudes in AAV-shCON mice were significantly higher than that of AAV-shTDP-43 mice under both LD and DD conditions, but with no significant difference in total motor activity between groups (Figure 4G). Lumicycle recordings of SCN slices expressing *Per2-luc* further confirmed these findings, as AAV-shCON mice maintained elegant cosine-wave oscillations of the *Per2* reporter expression while AAV-shTDP-43 in the SCN resulted in arrhythmicity (Figure 4H). These results clearly underscore the role of TDP-43 in maintaining the circadian rhythm of the SCN.

Recent studies illustrated that TDP-43 pathology is associated with hippocampal sclerosis, which correlates with cognitive decline observed in certain neurodegenerative diseases.²⁴ In addition, TDP-43^{Q331K} mice exhibited cognitive impairment and reduced locomotor behavior.²⁵ To explore whether TDP-43 knockdown in the hippocampus affects circadian rhythms similarly to the SCN, we bilaterally injected AAV-shTDP-43 into the CA1 region of the hippocampus in adult mice (Figure S3A). After three weeks, we assessed TDP-43 expression in the hippocampus via western blotting and immunofluorescence staining. As expected, TDP-43 expression was attenuated in AAV-shTDP-43 compared to AAV-shCON, as evidenced by immunoblotting and fluorescence staining (Figures S3B and S3C). However, locomotor activity



<i>JTK_Cycle</i>	<i>P_value</i>	<i>JTK_Cycle</i>	<i>P_value</i>
PER2	2.32E-06	CRY2	0.000588
	0.000827		1.35E-06
	1		0.154823
BMAL1	2.34E-07	TDP-43	7.73E-07
	0.000289		3.90E-06
	0.608139		0.259182
CRY1	1.35E-06	GAPDH	1
	9.16E-05		1
	1		0.711707

Figure 3. Disruption of TDP-43 impacts clock genes regulation

(A) Luciferase activity driven by E-box in HEK293 cells following transfection with varying amounts of TDP-43 or CRY1 expression vectors in a 96-well plate. $n = 3$ represents technical replicates.
 (B) Transient transfection luciferase assay demonstrating differential repression activity in shTDP-43 and shcon cells. $n = 3$ represents technical replicates.
 (C) mRNA levels of indicated clock genes in shTDP-43, shcon, and U2OS cells harvested every 4 h after synchronization (medium change). $n = 3$ samples per time point. The JTK_Cycle analysis was conducted to evaluate the rhythmicity of gene expression. $JTK_p < 0.05$ indicates significantly rhythmic.
 (D) Expression profiles of CLOCK, PER2, CRY1, and CRY2 in shTDP-43, shcon, and U2OS cells harvested every 4 h after synchronization (medium change). Bottom: JTK_Cycle analysis was conducted to evaluate the rhythmicity of gene expression. $JTK_p < 0.05$ indicates significantly rhythmic. One-way ANOVA with multiple comparison test for (A) and (B), two-way ANOVA with multiple comparison test for (C) and (D). Data are presented as mean \pm SEM, ns indicates no significance; * $p < 0.05$, ** $p < 0.01$, *** $p < 0.001$, **** $p < 0.0001$.

analysis revealed robust rhythmicity in both AAV-shTDP-43 and AAV-shCON mice, with no significant differences in period or locomotor activity (Figures S3D–S3F). In addition, we assessed the rhythmicity of SCN expressed *Per2-luc* that knocked down TDP-43 in the CA1 region of the hippocampus using Lumicycle recording, and the results showed no significant differences in period, amplitude, or phase between the two groups (Figure S3G). Thus, knockdown of TDP-43 in the CA1 region of the hippocampus cannot influence circadian rhythmicity in mammals.

Taken together, these findings confirm that disrupted TDP-43 in the SCN, instead of the hippocampus, induces irregular rhythms in mice. These results align with our observations of TDP-43 knockdown in U2OS cells, reinforcing the notion that TDP-43 plays a crucial role in regulating the circadian clock.

AAV-shTDP-43 mice display depression-like behavior

It has been reported that TDP-43 is primarily associated with neurodegenerative diseases, which are clinically characterized by symptoms such as apathy, loss of empathy, stubbornness, altered dietary patterns, and stereotypic behavior.²⁶ Approximately 50–60% of patients with FTD were previously diagnosed with major depressive disorder (MDD), and 20–30% were diagnosed with bipolar disorder (BD).²⁷ We hypothesized that depressive or manic behavior might serve as a prodromal symptom of FTD. To investigate this hypothesis, we assessed behavioral changes resulting from TDP-43 knockdown in the SCN or CA1 region of the hippocampus in males and females using a battery of tests, including the open field test (OPT), sucrose preference test (SPT), forced swimming test (FST), and tail suspension test (TST) (Figure 5A; Figure S4A).

In the group of mice with TDP-43 knockdown in the SCN, the OPT revealed that expressing AAV-shTDP-43 and those with AAV-shCON exhibited no significant differences in terms of total distance traveled, percentage of time in center and percentage of distance traveled in center zone (Figure 5B). In the SPT, we assessed sucrose preference ratios for both groups during two time intervals: ZT0-12 and ZT12-24. While there appeared to be a decrease in sucrose preference for AAV-shTDP-43 mice compared to AAV-shCON mice in ZT0-12, this difference did not reach statistical significance. However, during the period from ZT12 to ZT24, AAV-shTDP-43 mice exhibited a significant reduction in sucrose preference when compared to AAV-shCON mice (Figure 5C). Furthermore, analyses of the FST and TST demonstrated that AAV-shTDP-43 mice display a significantly higher percentage of total immobility compared to AAV-shCON mice (Figures 5D and 5E). These findings suggest that disruption of TDP-43 in the SCN can induce depressive behaviors in mice. In addition, we sought to examine whether TDP-43 deficiency in the CA1 region of the hippocampus resulted in similar behavioral outcomes (Figure S4A). However, in the group of mice with TDP-43 knockdown in the CA1 region of the hippocampus, there were no significant differences observed between AAV-shTDP-43 and AAV-shCON mice in the OPT, SPT, FST, and TST (Figures S4B–S4E).

Taken together, these data further support that disruption of TDP-43 in the SCN, but not in the hippocampus, can lead to depressive symptoms in mice. This may be attributed to the disruption of TDP-43 in the SCN, which subsequently results in dysregulation of core clock genes and disturbances in circadian rhythms, ultimately inducing prodromal symptoms of FTD in mice, including depression.

TDP-43 deficiency in SCN disrupts c-fos rhythm in prefrontal cortex

The expression of c-Fos often reflects neuronal activation and highlights circadian rhythms in different cerebral regions, including SCN, nucleus accumbens (NAc), amygdala, hippocampus, and medial prefrontal cortex (mPFC). Their diurnal rhythms of c-Fos are the key mediators for motivation and reward, while any disruption in the c-Fos rhythm can induce aberrant emotion responses.^{28–31} To investigate whether depressive-like behaviors resulting from TDP-43 loss in the SCN may be related to disrupted rhythms of neural activity in depression-related brain regions, we conducted a time course of c-Fos expressions in brain regions associated with depression, including the prefrontal cortex (PFC), amygdala, hippocampus, and NAc.^{32,33} Immunofluorescent staining revealed significant diurnal rhythms of c-Fos activation in the PFC region of AAV-shCON mice, with a trough at ZT8 and peaks at ZT20. However, no such rhythmicity was observed in PFC of AAV-shTDP-43 mice (Figures 6A and 6B). Consistent with these results, time course qPCR analysis of *c-fos* mRNA levels showed no rhythmicity in PFC of AAV-shTDP-43 mice, but exhibited robust rhythmicity in PFC of AAV-shCON mice (Figure S5). In contrast to the PFC, loss of TDP-43 in SCN did not obviously affect c-Fos rhythmicity in other depression-related brain regions, including the amygdala, hippocampus, and NAc. In the NAc, the c-Fos expression in both AAV-shCON and AAV-shTDP-43 mice peaked at ZT 20–24 and had a trough at ZT8–12, which consistent with the rhythmic pattern in the PFC of control mice, whereas c-Fos rhythms in hippocampus and amygdala displayed an inverse rhythmic pattern, with peaks from ZT4–8 and nadirs from ZT16–20 (Figures 6C–6E). These findings suggested that TDP-43 knockdown in SCN could disrupt

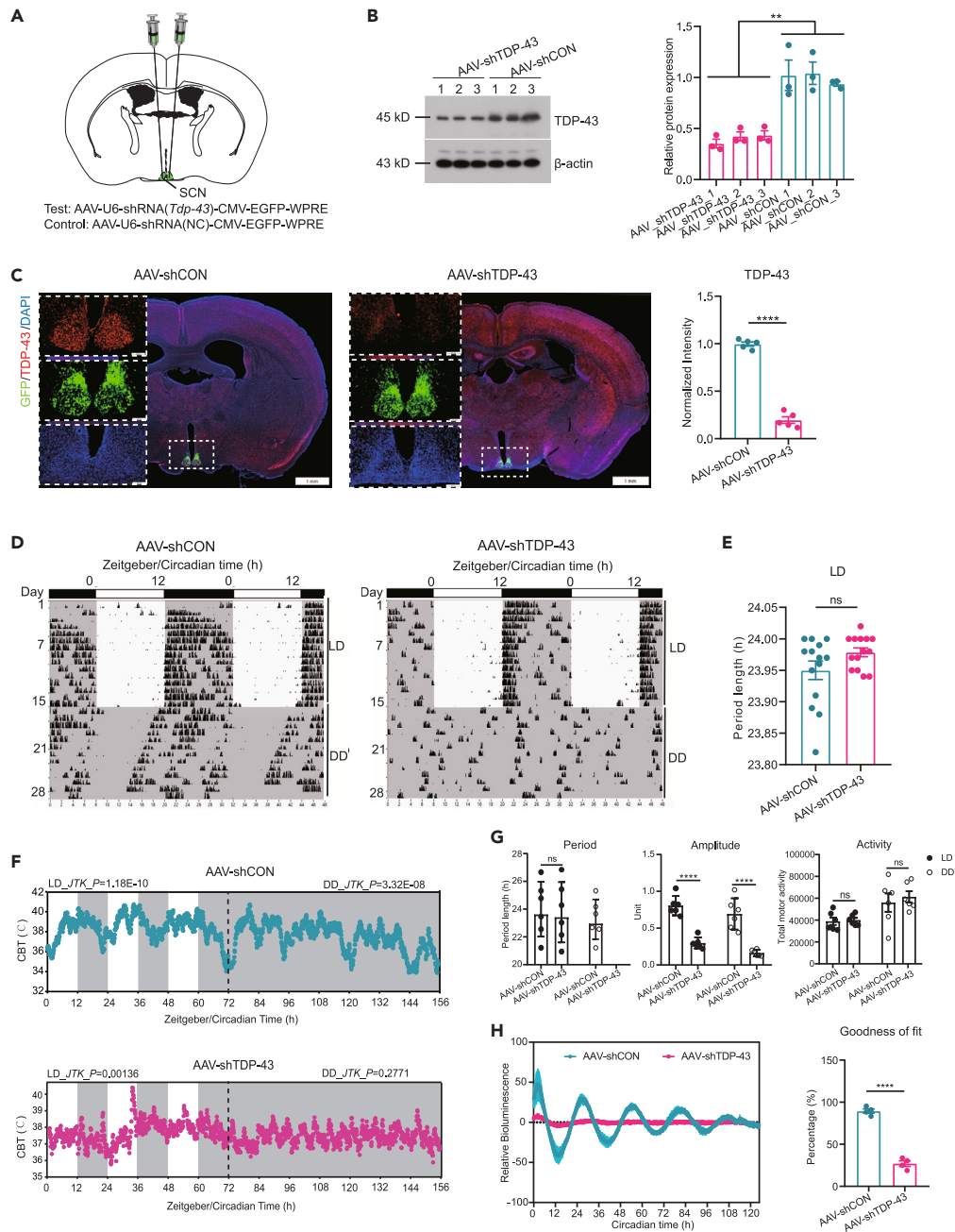


Figure 4. TDP-43 oscillation plays a dominant role in circadian rhythm of mammals

(A) Schematic diagram showing stereotaxic injection of AAV expressing shTDP-43 and shCON into the SCN of the hypothalamus.
 (B) Western blots depicting TDP-43 levels in the hypothalamus of male and female mice expressing shCON or shTDP-43 following AAV infection for three weeks. Right: Statistical analysis of protein levels. $n = 3$ samples per group.
 (C) Immunofluorescence staining of the TDP-43 protein in SCN infected with AAV-shCON or AAV-shTDP-43 males and females. The dotted line indicates the SCN. Immunostained slices (40 μ m thickness per slice) were stained with DAPI (blue) and TDP-43 (red) antibody, Green: green fluorescent protein (GFP). $n = 5$ mice per group. Scale bar, 1 mm. Left insert: zoom-in on the SCN region. Scale bar, 100 μ m. Right: Quantitative analysis of TDP-43 expression in the SCN. The intensity of TDP-43 normalized to the intensity of the control group.
 (D) Double-plotted actograms showing wheel-running activity for AAV-shCON and AAV-shTDP-43 male mice. Vertical black marks represent activity counts. Gray indicates dark phase; white indicates light phase. Day 1–14 depicts entrainment to an LD cycle; activity occurs in regular 24-h cycle and primarily during darkness. Day 15–28 depicts behavior under DD condition, in which free-running periods are less than 24 h and activity begins slightly earlier each day. $n = 14$ mice per group.
 (E) Histogram of the period for AAV-shCON and AAV-shTDP-43 mice in LD 12:12 h detected in (D).

Figure 4. Continued

(F) Longitudinal recording of core body temperature (CBT) in AAV-shCON and AAV-shTDP-43 mice. Mice were exposed to LD cycle for three days, followed by constant DD condition for three days. Gray areas indicate dark phase; white areas indicate light phase. Values obtained by BD2eJTK analysis are shown in each subpanel. $JTK_P < 0.01$ indicates significantly rhythmic. $n = 6$ mice per group (3 males and 3 females).

(G) Analysis of circadian rhythms detected in (F), including period (left), amplitude (middle) and motor activity (right) between LD and DD phases.

(H) Representative *Per2-luc* rhythms in ex vivo cultured SCN explants from AAV-shCON or AAV-shTDP-43 male mice. Right: Rhythmicity analyses of robustness for SCN explants from AAV-shCON or AAV-shTDP-43 mice. $n = 4$ samples per group. Unpaired two-tailed t-test for two group comparisons in (B), (C), (E), and (H). two-way ANOVA with multiple comparison test for (G). Data are presented as mean \pm SEM, ns indicates no significance; * $p < 0.05$, ** $p < 0.01$, *** $p < 0.001$, **** $p < 0.0001$.

rhythmic activation by c-Fos in the PFC, but not amygdala, hippocampus, or NAc, and this disruption was accompanied by depressive-like behaviors in mice.

Given that mice with *Tdp-43* knockdown in the hippocampus didn't exhibit depression-like behavior, while their c-Fos expression may also exhibit an arrhythmic pattern in PFC, amygdala, hippocampus, or NAc regions, we then injected AAV-TDP-43 or AAV-shCON in the hippocampus of C57BL/6J mice and measured immunofluorescent signal of c-Fos in the PFC of mice at anti-phased time points (ZT8 and ZT20). We found that knockdown of TDP-43 in hippocampus resulted in no significant differences in c-Fos expressions in PFC between AAV-shCON and AAV-shTDP-43 at either ZT8 or ZT20 (Figures S6A and S6B). Simultaneously, we also assessed c-Fos signaling in other depression-related brain regions, including the amygdala, hippocampus, and NAc. Immunofluorescence analysis indicated that there were no significant differences in c-Fos expressions in these brain regions between AAV-shTDP-43 and AAV-shCON (Figures S6C–S6E). These data clearly suggest that the loss of TDP-43 in the hippocampus did not induce differential rhythmic expression of c-Fos in these brain regions.

Taken together, these findings support the idea that TDP-43 loss in the SCN induces arrhythmic locomotor activity and depressive behavior through abnormal rhythm of c-Fos activity specifically in the PFC, while TDP-43 deficiency in the hippocampus does not elicit such responses in these brain regions.

DISCUSSION

Our study has unveiled a compelling connection between the ALS/FTD-associated gene TDP-43, disruptions in circadian rhythmicity, and the potential role of TDP-43 in depressive disorders, which may serve as a prodromal symptom of FTD. We embarked on this investigation by initially identifying TDP-43 as a gene exhibiting rhythmic expression patterns. Subsequently, we provided compelling evidences that the knockdown of TDP-43 disrupts the intricate regulation of core clock genes, ultimately leading to arrhythmicity. Furthermore, our experiments in mice, where we confirmed that TDP-43 interference significantly affects circadian regulation, underscore the crucial role of TDP-43 in governing the circadian clock. Importantly, mice expressing AAV-TDP-43 in the SCN exhibited increased depression-like behavior. These findings resonate with clinical observations where sleep-wake disturbances are commonly noted in neurodegenerative diseases, and depression often emerges as an early sign of FTD.^{27,34} Moreover, prior mouse model studies have demonstrated that unpredictable chronic mild stress can reduce the amplitude of circadian activity and body temperature, and the disruption of clock rhythmicity or mutations in clock genes can induce depression-like behavior in mice.^{35,36} Our findings thus consolidate the intricate link between circadian rhythms, mood disorders, and neurodegenerative diseases.

Notably, previous research has established TDP-43 proteinopathy in sleep-related brain regions, with sleep-wake disturbances being a prevalent phenomenon in neurodegenerative diseases.^{37,38} Sleep-wake cycles play a crucial role in the regulation of protein homeostasis in the brain. Prolonged wakefulness or sleep deprivation can elevate protein translation factors associated with the unfolded protein response (UPR) pathway, which governs protein homeostasis by overseeing processes such as protein synthesis, degradation, and folding. Notably, the integrated stress response downstream of the UPR activates the autophagy pathway, inducing protein aggregation and facilitating the degradation of defective organelles.³⁹ However, diminished autophagy facilitates the aggregation of TDP-43/FUS, forming a permanent toxic loop.⁴⁰ Additionally, modifying sleep and feeding rhythms in mice results in the desynchronization of clock gene oscillations between the SCN and hippocampus, consequently causing significant disruptions in learning and memory.⁴¹ Moreover, sleep deprivation significantly expedites the deposition of amyloid plaques in Alzheimer's disease (AD) patients, as well as exacerbates tau pathology and dendritic spine loss in AD mice.^{42,43} This suggests the involvement of circadian rhythms in ALS and FTD pathogenesis. However, the mechanistic connection between circadian rhythms and neurodegenerative diseases, as well as the specific functions of TDP-43 in this context, remained elusive. Our work has revealed that TDP-43 knockdown disrupted the core transcriptional activation governing circadian rhythms. Additionally, it lowered the expression levels of *CLOCK* and *BMAL1* through its post-transcriptional regulation, resulting in decreased expression of downstream clock genes. Moreover, the find of arrhythmic *Tdp-43* in *Bmal1*^{-/-} and *Cry1*^{-/-} mouse fibroblast cells indicated the disruption of core circadian clock genes might also affect the circadian rhythm of TDP-43 expression (Figure S7), which suggests that normal circadian rhythms and expression of clock genes require the participation of intact TDP-43 and circadian clock genes. Furthermore, we observed that the loss of TDP-43 in the SCN, but not the hippocampus, induces locomotion arrhythmicity, reduced locomotor activity, and depressive-like behavior in mice.

Moreover, it's worth noting that patients with TDP-43 pathology often exhibit hippocampal damage and severe cognitive decline. Consistent with these clinical observations, mice with hippocampal loss of TDP-43 showed cognitive dysfunction.^{44–46} However, in our study, we did not observe depression-like behavior in mice expressing AAV-shTDP-43 in the hippocampus. This suggests that the role of TDP-43 in mood regulation may be more pronounced in the SCN and highlights the region-specific effects of TDP-43 deficiency.

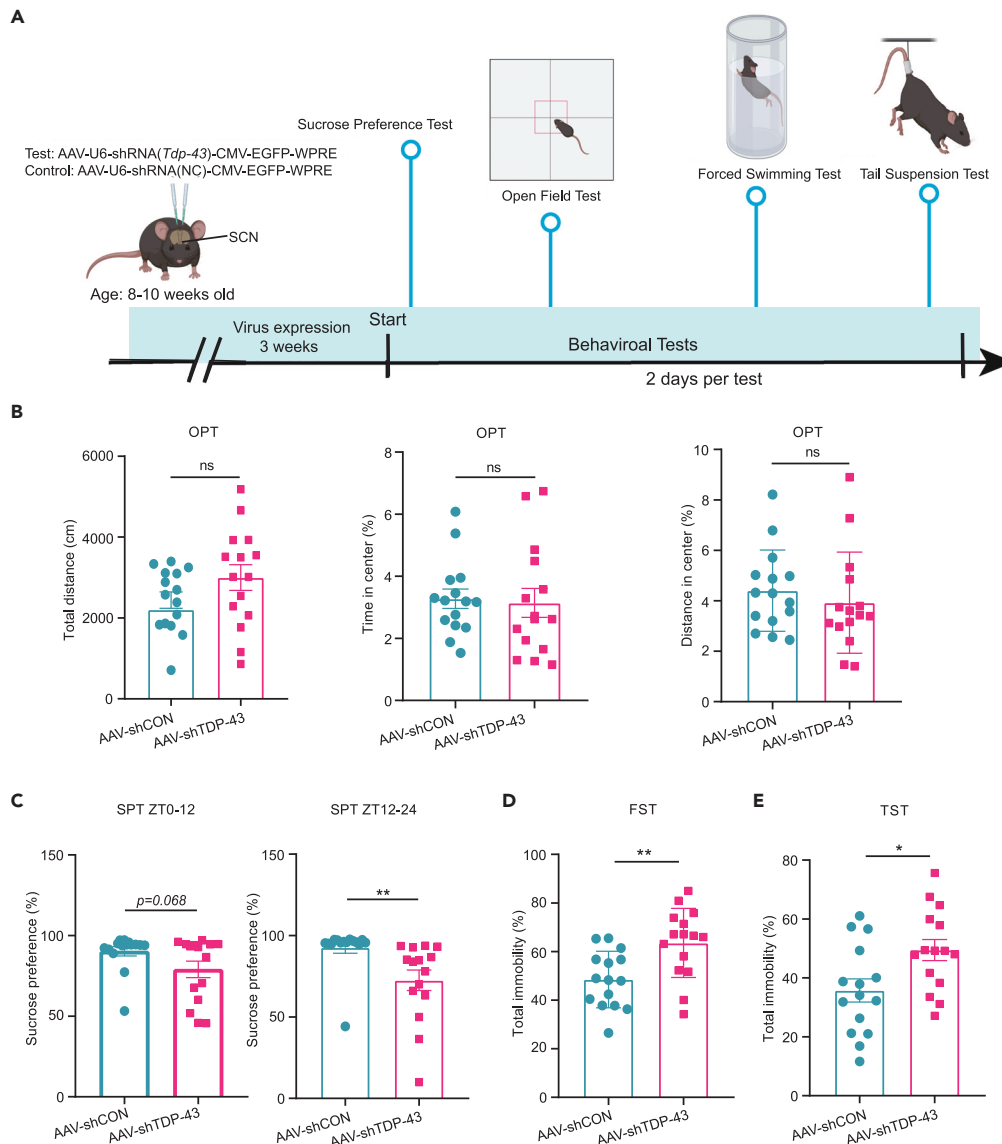


Figure 5. AAV-shTDP-43 in SCN induces depression-like behavior

(A) Schematic diagram showing the timeline for stereotactic injection of AAV expressing shCON and shTDP-43 into the SCN of the hypothalamus followed by behavioral tests.

(B) Results of open field test, including total distance traveled (left) and percentage of time in center (middle) and percentage of distance traveled in center (right). Recording time was 5 min.

(C) Percentage of sucrose preference during ZT0 -12 (left) or ZT12- 24 (right).

(D) Percentage of immobility time in the forced swimming test, with the time recorded in the last 4 out of 6 min.

(E) Percentage of immobility time in the Tail Suspension Test, with the time recorded in the last 4 out of 6 min. Unpaired two-tailed t-test for two group comparisons in (B)–(E). Data are presented as mean \pm SEM, the n of all data are 15 mice per group (10 males and 5 females), ns indicates no significance; * $p < 0.05$, ** $p < 0.01$.

In mammals, the SCN functions as the primary circadian pacemaker, and changes in circadian clock gene rhythmicity that can be observed in the paraventricular nucleus (PVN), PFC, rostral agranular insula, amygdala, and hippocampus support the likelihood that clock gene expressions in SCN has brain-wide effects on neural activity.⁴⁷ It should also be noted that stimulating SCN neurons results in activation of their cortical-projecting regions,⁴⁸ such as SCN regulation of clock gene expressions in paraventricular thalamus (PVT), NAC, or mPFC, which ultimately modulates daily cycles of dopaminergic transmission. Given this prior understanding, it is reasonable to propose that the SCN could regulate the accumulation of proteins required for dopaminergic signaling, innervating dopaminergic brain regions to induce changes in activity in these regions dependent on time-of-day. Thus, defects or deterioration of the SCN can impair rhythmic cycles in dopamine

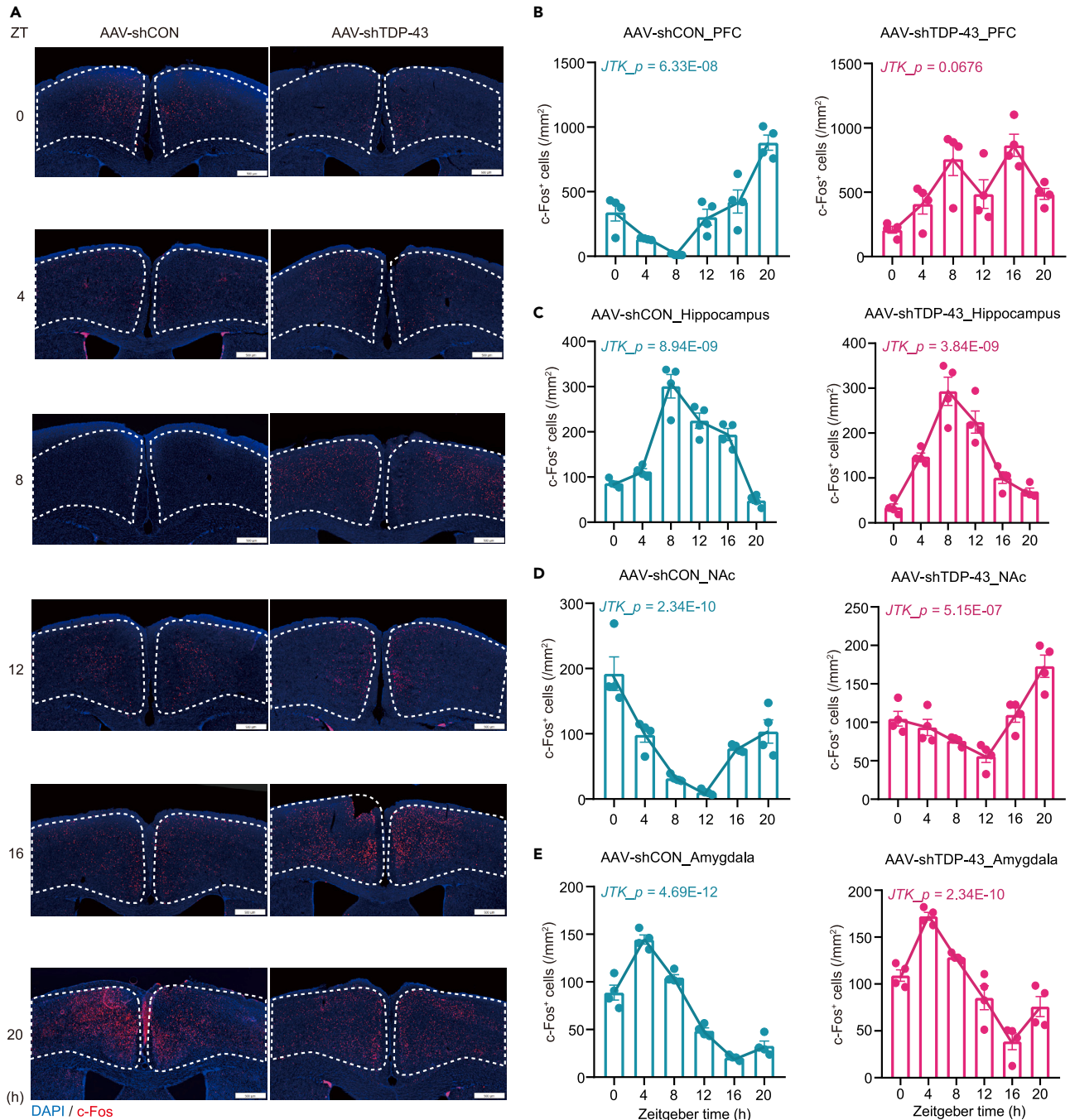


Figure 6. Loss of TDP-43 in SCN alters the diurnal rhythm of c-Fos in PFC

(A) Immunofluorescence staining of the c-Fos proteins in the brains of male mice infected with AAV-shCON or AAV-shTDP-43. The dotted line indicates the representative images of c-Fos⁺ cells over DAPI in PFC regions for a 24 h cycle. Slices were stained with DAPI (blue) and c-Fos (red) antibody. 8 PFC sections per mouse and $n = 4$ mice for each time point. Scale bar, 500 μ m.

(B) Quantification of c-Fos⁺ cells overlaid on the DAPI in PFC regions detected in (A).

(C–E) Quantification of c-Fos⁺ cells overlaid on the DAPI signals in hippocampus, NAc and amygdala regions of male mice for a 24 h cycle, respectively. 8 sections per mouse and $n = 4$ mice for each time point. JTK_Cycle analysis was conducted to evaluate c-Fos expression rhythmicity in PFC, hippocampus, NAc and amygdala. $JTK_p < 0.05$ indicates significantly rhythmic. All data are presented as mean \pm SEM.

transporter (DAT) protein levels, altering responses to reward mediated by SCN—PVT—mPFC projections.⁴⁹ Furthermore, the rhythmicities of immediate-early gene expressions (e.g., *IEGs*, *Fos*, *Egr1*, *Arc*) in the PFC are disrupted in mice with chronic exposure to reversed light-dark cycle, resulting in anxiety-like behaviors.⁵⁰ Previous studies have shown that c-Fos in the NAc and mPFC regions is rhythmically expressed, reaching the highest in the active phase (ZT18) and the lowest during the rest phase (ZT10). In contrast, the circadian expression of c-Fos in the hippocampus displays the inverse rhythmic pattern. This rhythmic neural activation may contribute to the circadian regulation of emotion-related behaviors.^{29,31} However, our study revealed that TDP-43 knockdown in SCN led to arrhythmic expression of c-Fos in PFC. This finding might suggest that TDP-43 deficiency disrupts the circadian pattern of c-Fos in the PFC, potentially contributing to depression-like behaviors. These findings have significant clinical implications, particularly considering the overlap between psychiatric disorders and ALS/FTD.

Previous research has indicated that psychiatric disorders are prevalent among ALS patients, often emerging within 1–5 years after the initial ALS diagnosis.^{51–54} This underscores the intricate interplay between psychiatric conditions and ALS/FTD and suggests a shared pathophysiological basis. Several studies may explain the link between depression and dementia. It is possible that psychiatric disorders, including depression contribute to dementia, involving the hyperactivity of the hypothalamic-pituitary-adrenal (HPA) axis and a decline in metabolic capacity of brain cells.^{55,56} Alternatively, dementia-related cognitive, behavioral and lifestyle changes precipitate the onset of depression.^{57,58} In addition, mood stabilizers like lithium, commonly used to treat mood disorders, have shown promise in improving symptoms in ALS/FTD patients, particularly in ALS patients with variants of the UNC13 presynaptic protein.^{18,59} Moreover, light therapy could normalize melatonin secretion in FTD patients and effectively treat sleep-wake and behavioral activity disorders in these patients. This suggests that the regulation of circadian rhythms can play a significant role in mitigating the symptoms of FTD.^{60,61}

In summary, our study has established a compelling link between mood disorders and neurodegenerative disorders, shedding light on the specific brain regions responsible for behavioral disturbances and highlighting the critical role of TDP-43 in circadian regulation. These findings hold promise for future clinical treatment strategies for ALS/FTD.

Limitations of the study

While our study provides valuable insights, it is not without limitations. First and foremost, our investigation primarily focused on assessing anxiety and depression behaviors in mice, without encompassing variations in cognitive behaviors. Cognitive deficits are significant components of neurodegenerative diseases, and future research should aim to address these aspects comprehensively. Secondly, we did not measure the molecular markers associated with ALS/FTD in our mouse models or in individuals with mental illness disorders. This aspect warrants further exploration to establish a more comprehensive understanding of the intricate links between the circadian clock and mental and neurodegenerative diseases. Future research endeavors should aim to bridge these gaps and provide a more holistic perspective on these complex relationships.

STAR★METHODS

Detailed methods are provided in the online version of this paper and include the following:

- KEY RESOURCES TABLE
- RESOURCE AVAILABILITY
 - Lead contact
 - Materials availability
 - Data and code availability
- EXPERIMENTAL MODEL AND STUDY PARTICIPANT DETAILS
 - Animal procedures
- METHOD DETAILS
 - Cell culture
 - Plasmids construction and stable cell line generation
 - Luciferase assay
 - Quantitative real-time PCR (qRT-PCR) analysis
 - Western blotting
 - Immunofluorescent staining
 - Stereotactic virus injection
 - Bioluminescence rhythms in cell and tissue culture
 - Wheel-running analysis
 - Core body temperature recording
 - Behavioral analyses
- QUANTIFICATION AND STATISTICAL ANALYSIS

SUPPLEMENTAL INFORMATION

Supplemental information can be found online at <https://doi.org/10.1016/j.isci.2024.109522>.

ACKNOWLEDGMENTS

We thank Dr. Ziqing Yu and Di Sang in E.E.Z.'s lab for technical support and scientific inputs. The research was supported by the funds from Ministry of Science and Technology of the People's Republic of China (2021ZD0203400 to E.E.Z.), National Natural Science Foundation of China (31971090 to E.E.Z. and 32060040 to X.H.), Jiangxi Natural Science Foundation (20202BAB206062 to X.H.), and Double-Thousand Talents Program of Jiangxi Province (JXSQ2023201019 to X.H.).

AUTHOR CONTRIBUTIONS

H.Z., X.H., and E.E.Z. conceived the study. H.Z., X.H., and E.E.Z. designed the experiments. H.Z. performed the molecular/cellular experiments; H.Z. and C.C. performed the mouse work; H.Z. analyzed all other experimental results. E.E.Z. oversaw the project. H.Z., E.E.Z., and X.H. wrote the manuscript, which all authors commented on.

DECLARATION OF INTERESTS

The authors declare no competing interests.

Received: September 25, 2023

Revised: December 28, 2023

Accepted: March 14, 2024

Published: March 16, 2024

REFERENCES

- Albrecht, U. (2012). Timing to perfection: the biology of central and peripheral circadian clocks. *Neuron* 74, 246–260. <https://doi.org/10.1016/j.neuron.2012.04.006>.
- Takahashi, J.S., Hong, H.-K., Ko, C.H., and McDearmon, E.L. (2008). The genetics of mammalian circadian order and disorder: implications for physiology and disease. *Nat. Rev. Genet.* 9, 764–775. <https://doi.org/10.1038/nrg2430>.
- Gekakis, N., Staknis, D., Nguyen, H.B., Davis, F.C., Wilsbacher, L.D., King, D.P., Takahashi, J.S., and Weitz, C.J. (1998). Role of the CLOCK protein in the mammalian circadian mechanism. *Science (New York, N.Y.)* 280, 1564–1569. <https://doi.org/10.1126/science.280.5369.1564>.
- Zhang, E.E., and Kay, S.A. (2010). Clocks not winding down: unravelling circadian networks. *Nat. Rev. Mol. Cell Biol.* 11, 764–776. <https://doi.org/10.1038/nrm2995>.
- Kume, K., Zylka, M.J., Sriram, S., Shearman, L.P., Weaver, D.R., Jin, X., Maywood, E.S., Hastings, M.H., and Reppert, S.M. (1999). mCRY1 and mCRY2 are essential components of the negative limb of the circadian clock feedback loop. *Cell* 98, 193–205. [https://doi.org/10.1016/S0092-8674\(00\)81014-4](https://doi.org/10.1016/S0092-8674(00)81014-4).
- Siepk, S.M., Yoo, S.-H., Park, J., Song, W., Kumar, V., Hu, Y., Lee, C., and Takahashi, J.S. (2007). Circadian mutant Overtime reveals F-box protein FBXL3 regulation of cryptochrome and period gene expression. *Cell* 129, 1011–1023. <https://doi.org/10.1016/j.cell.2007.04.030>.
- Videnovic, A., Lazar, A.S., Barker, R.A., and Overeem, S. (2014). 'The clocks that time us'—circadian rhythms in neurodegenerative disorders. *Nat. Rev. Neurol.* 10, 683–693. <https://doi.org/10.1038/nrneurol.2014.206>.
- Buratti, E., and Baralle, F.E. (2012). TDP-43: gumming up neurons through protein–protein and protein–RNA interactions. *Trends Biochem. Sci.* 37, 237–247. <https://doi.org/10.1016/j.tibs.2012.03.003>.
- Arai, T., Hasegawa, M., Akiyama, H., Ikeda, K., Nonaka, T., Mori, H., Mann, D., Tsuchiya, K., Yoshida, M., Hashizume, Y., and Oda, T. (2006). TDP-43 is a component of ubiquitin-positive tau-negative inclusions in frontotemporal lobar degeneration and amyotrophic lateral sclerosis. *Biochem. Biophys. Res. Commun.* 351, 602–611. <https://doi.org/10.1016/j.bbrc.2006.10.093>.
- Sreedharan, J., Blair, I.P., Tripathi, V.B., Hu, X., Vance, C., Rogelj, B., Ackerley, S., Durnall, J.C., Williams, K.L., Buratti, E., et al. (2008). TDP-43 mutations in familial and sporadic amyotrophic lateral sclerosis. *Science (New York, N.Y.)* 319, 1668–1672. <https://doi.org/10.1126/science.1154584>.
- Benajiba, L., Le Ber, I., Camuzat, A., Lacoste, M., Thomas-Anterion, C., Couratier, P., Legallic, S., Salachas, F., Hannequin, D., Decousus, M., et al. (2009). TARDBP mutations in motoneuron disease with frontotemporal lobar degeneration. *Ann. Neurol.* 65, 470–473. <https://doi.org/10.1002/ana.21612>.
- Anderson, K.N., Hatfield, C., Kipps, C., Hastings, M., and Hodges, J.R. (2009). Disrupted sleep and circadian patterns in frontotemporal dementia. *Eur. J. Neurol.* 16, 317–323. <https://doi.org/10.1111/j.1468-1331.2008.02414.x>.
- Mishima, K., Tozawa, T., Satoh, K., Matsumoto, Y., Hishikawa, Y., and Okawa, M. (1999). Melatonin secretion rhythm disorders in patients with senile dementia of Alzheimer's type with disturbed sleep–waking. *Biol. Psychiatr.* 45, 417–421. [https://doi.org/10.1016/s0006-3223\(97\)00510-6](https://doi.org/10.1016/s0006-3223(97)00510-6).
- Stopa, E.G., Volicer, L., Kuo-Leblanc, V., Harper, D., Lathi, D., Tate, B., and Satlin, A. (1999). Pathologic evaluation of the human suprachiasmatic nucleus in severe dementia. *J. Neuropathol. Exp. Neurol.* 58, 29–39. <https://doi.org/10.1097/00005072-199901000-00004>.
- Patacchioli, F.R., Monnazzi, P., Scontrini, A., Tremante, E., Caridi, I., Brunetti, E., Buttarelli, F.R., and Pontieri, F.E. (2003). Adrenal dysregulation in amyotrophic lateral sclerosis. *J. Endocrinol. Invest.* 26, RC23–RC25. <https://doi.org/10.1007/BF03349149>.
- Huang, Z., Liu, Q., Peng, Y., Dai, J., Xie, Y., Chen, W., Long, S., Pei, Z., Su, H., and Yao, X. (2018). Circadian rhythm dysfunction accelerates disease progression in a mouse model with amyotrophic lateral sclerosis. *Front. Neurol.* 9, 218. <https://doi.org/10.3389/fneur.2018.00218>.
- Nascimento, C., Nunes, V.P., Diehl Rodriguez, R., Takada, L., Suemoto, C.K., Grinberg, L.T., Nitirini, R., Lafer, B., and Psychiatry, B. (2019). A review on shared clinical and molecular mechanisms between bipolar disorder and frontotemporal dementia. *Prog. Neuro-Psychopharmacol. Biol. Psychiatry* 93, 269–283. <https://doi.org/10.1016/j.pnpb.2019.04.008>.
- Limanaqi, F., Biagioni, F., Ryskalin, L., Busceti, C.L., and Fornai, F. (2019). Molecular mechanisms linking ALS/FTD and psychiatric disorders, the potential effects of lithium. *Front. Cell. Neurosci.* 13, 450. <https://doi.org/10.3389/fncel.2019.00450>.
- Ju, D., Zhang, W., Yan, J., Zhao, H., Li, W., Wang, J., Liao, M., Xu, Z., Wang, Z., Zhou, G., et al. (2020). Chemical perturbations reveal that RUVBL2 regulates the circadian phase in mammals. *Sci. Transl. Med.* 12, eaba0769. <https://doi.org/10.1126/scitranslmed.aba0769>.
- Hirano, A., Nakagawa, T., Yoshitane, H., Oyama, M., Kozuka-Hata, H., Lanjakornsiripan, D., and Fukada, Y. (2016). USP7 and TDP-43: pleiotropic regulation of cryptochrome protein stability paces the oscillation of the mammalian circadian clock. *PLoS One* 11, e0154263. <https://doi.org/10.1371/journal.pone.0154263>.
- Zhang, E.E., Liu, A.C., Hirota, T., Miraglia, L.J., Welch, G., Pongsawakul, P.Y., Liu, X., Atwood, A., Huss, J.W., 3rd, Janes, J., et al. (2009). A genome-wide RNAi screen for modifiers of the circadian clock in human cells. *Cell* 139, 199–210. <https://doi.org/10.1016/j.cell.2009.08.031>.
- Buratti, E., and Baralle, F.E. (2010). The multiple roles of TDP-43 in pre-mRNA processing and gene expression regulation.

- RNA Biol. 7, 420–429. <https://doi.org/10.4161/ma.7.4.12205>.
23. Zielinski, T., Moore, A.M., Troup, E., Halliday, K.J., and Millar, A.J. (2014). Strengths and limitations of period estimation methods for circadian data. *PLoS One* 9, e96462. <https://doi.org/10.1371/journal.pone.0096462>.
 24. Aoki, N., Murray, M.E., Ogaki, K., Fujioka, S., Rutherford, N.J., Rademakers, R., Ross, O.A., and Dickson, D.W. (2015). Hippocampal sclerosis in Lewy body disease is a TDP-43 proteinopathy similar to FTLTDP Type A. *Acta Neuropathol.* 129, 53–64. <https://doi.org/10.1007/s00401-014-1358-z>.
 25. White, M.A., Kim, E., Duffy, A., Adalbert, R., Phillips, B.U., Peters, O.M., Stephenson, J., Yang, S., Massenzio, F., Lin, Z., et al. (2018). TDP-43 gains function due to perturbed autoregulation in a Tardbp knock-in mouse model of ALS-FTD. *Nat. Neurosci.* 21, 552–563. <https://doi.org/10.1038/s41593-018-0113-5>.
 26. Rascovsky, K., Hodges, J.R., Knopman, D., Mendez, M.F., Kramer, J.H., Neuhaus, J., Van Swieten, J.C., Seelaar, H., Dopper, E.G.P., Onyike, C.U., et al. (2011). Sensitivity of revised diagnostic criteria for the behavioural variant of frontotemporal dementia. *Brain* 134, 2456–2477. <https://doi.org/10.1093/brain/awr179>.
 27. Ichikawa, T., Baba, H., Maeshima, H., Shimano, T., Inoue, M., Ishiguro, M., Yasuda, S., Shukuzawa, H., Suzuki, T., and Arai, H. (2019). Serum levels of TDP-43 in late-life patients with depressive episode. *J. Affect. Disord.* 250, 284–288. <https://doi.org/10.1016/j.jad.2019.03.024>.
 28. Velazquez, F.N., Caputto, B.L., and Boussin, F.D. (2015). c-Fos importance for brain development. *Aging (Albany NY)* 7, 1028–1029. <https://doi.org/10.18632/aging.100862>.
 29. Kononen, J., Koistinaho, J., and Alho, H. (1990). Circadian rhythm in c-fos-like immunoreactivity in the rat brain. *Neurosci. Lett.* 120, 105–108. [https://doi.org/10.1016/0304-3940\(90\)90179-d](https://doi.org/10.1016/0304-3940(90)90179-d).
 30. Robins, M.T., Li, J., and Ryabinin, A.E. (2020). Effects of Housing Conditions and Circadian Time on Baseline c-Fos Immunoreactivity in C57BL/6J Mice. *Neuroscience* 431, 143–151. <https://doi.org/10.1016/j.neuroscience.2020.02.006>.
 31. Baltazar, R.M., Coolen, L.M., and Webb, I.C. (2013). Diurnal rhythms in neural activation in the mesolimbic reward system: critical role of the medial prefrontal cortex. *Eur. J. Neurosci.* 38, 2319–2327. <https://doi.org/10.1111/ejn.12224>.
 32. Krishnan, V., and Nestler, E.J. (2008). The molecular neurobiology of depression. *Nature* 455, 894–902. <https://doi.org/10.1038/nature07455>.
 33. Pandya, M., Altinay, M., Malone, D.A., and Anand, A. (2012). Where in the brain is depression? *Curr. Psychiatr. Rep.* 14, 634–642. <https://doi.org/10.1007/s11920-012-0322-7>.
 34. Barthlen, G.M., and Lange, D.J. (2000). Unexpectedly severe sleep and respiratory pathology in patients with amyotrophic lateral sclerosis. *Eur. J. Neurol.* 7, 299–302. <https://doi.org/10.1046/j.1468-1331.2000.00044.x>.
 35. Logan, R.W., Edgar, N., Gillman, A.G., Hoffman, D., Zhu, X., and McClung, C.A. (2015). Chronic stress induces brain region-specific alterations of molecular rhythms that correlate with depression-like behavior in mice. *Biol. Psychiatr.* 78, 249–258. <https://doi.org/10.1016/j.biopsych.2015.01.011>.
 36. Charrier, A., Olliac, B., Roubertoux, P., and Tordjman, S. (2017). Clock genes and altered sleep–wake rhythms: their role in the development of psychiatric disorders. *Int. J. Mol. Sci.* 18, 938. <https://doi.org/10.3390/ijms18050938>.
 37. Calderón-Garcidueñas, L., Rajkumar, R.P., Stommel, E.W., Kulesza, R., Mansour, Y., Rico-Villanueva, A., Flores-Vázquez, J.O., Brito-Aguilar, R., Ramírez-Sánchez, S., García-Alonso, G., et al. (2021). Brainstem quadruple aberrant hyperphosphorylated tau, beta-amyloid, alpha-synuclein and TDP-43 pathology, stress and sleep behavior disorders. *Int. J. Environ. Res. Publ. Health* 18, 6689. <https://doi.org/10.3390/ijerph18136689>.
 38. Wang, X., Wang, R., and Li, J. (2022). Influence of sleep disruption on protein accumulation in neurodegenerative diseases. *Ageing Neurodegener. Dis.* 2. <https://doi.org/10.20517/and.2021.10>.
 39. Hafycz, J.M., and Naidoo, N.N. (2019). Sleep, aging, and cellular health: Aged-related changes in sleep and protein homeostasis converge in neurodegenerative diseases. *Front. Aging Neurosci.* 11, 140. <https://doi.org/10.3389/fnagi.2019.00140>.
 40. Webster, C.P., Smith, E.F., Shaw, P.J., and De Vos, K.J. (2017). Protein homeostasis in amyotrophic lateral sclerosis: therapeutic opportunities? *Front. Mol. Neurosci.* 10, 123. <https://doi.org/10.3389/fnmol.2017.00123>.
 41. Loh, D.H., Jami, S.A., Flores, R.E., Truong, D., Ghiani, C.A., O'Dell, T.J., and Colwell, C.S. (2015). Misaligned feeding impairs memories. *Elife* 4, e09460. <https://doi.org/10.7554/eLife.09460>.
 42. Musiek, E.S., and Holtzman, D.M. (2016). Mechanisms linking circadian clocks, sleep, and neurodegeneration. *Science (New York, N.Y.)* 354, 1004–1008. <https://doi.org/10.1126/science.aah4968>.
 43. Morrone, C.D., Raghuraman, R., Hussaini, S.A., and Yu, W.H. (2023). Proteostasis failure exacerbates neuronal circuit dysfunction and sleep impairments in Alzheimer's disease. *Mol. Neurodegener.* 18, 27. <https://doi.org/10.1186/s13024-023-00617-4>.
 44. Wilson, A.C., Dugger, B.N., Dickson, D.W., Wang, D.S., and pathology, E. (2011). TDP-43 in aging and Alzheimer's disease—a review. *Int. J. Clin. Exp. Pathol.* 4, 147–155.
 45. Josephs, K.A., Whitwell, J.L., Weigand, S.D., Murray, M.E., Tosakulwong, N., Liesinger, A.M., Petrucelli, L., Senjem, M.L., Knopman, D.S., Boeve, B.F., et al. (2014). TDP-43 is a key player in the clinical features associated with Alzheimer's disease. *Acta Neuropathol.* 127, 811–824. <https://doi.org/10.1007/s00401-014-1269-z>.
 46. Ni, J., Ren, Y., Su, T., Zhou, J., Fu, C., Lu, Y., Li, D., Zhao, J., Li, Y., Zhang, Y., et al. (2023). Loss of TDP-43 function underlies hippocampal and cortical synaptic deficits in TDP-43 proteinopathies. *Mol. Psychiatr.* 28, 931–945. <https://doi.org/10.1038/s41380-021-01346-0>.
 47. Chun, L.E., Woodruff, E.R., Morton, S., Hinds, L.R., and Spencer, R.L. (2015). Variations in phase and amplitude of rhythmic clock gene expression across prefrontal cortex, hippocampus, amygdala, and hypothalamic paraventricular and suprachiasmatic nuclei of male and female rats. *J. Biol. Rhythm.* 30, 417–436.
 48. Liu, D., Li, J., Wu, J., Dai, J., Chen, X., Huang, Y., Zhang, S., Tian, B., and Mei, W. (2020). Monochromatic blue light activates suprachiasmatic nucleus neuronal activity and promotes arousal in mice under sevoflurane anesthesia. *Front. Neural Circ.* 14, 55. <https://doi.org/10.3389/fncir.2020.00055>.
 49. Sleipness, E.P., Sorg, B.A., and Jansen, H.T. (2007). Diurnal differences in dopamine transporter and tyrosine hydroxylase levels in rat brain: dependence on the suprachiasmatic nucleus. *Brain Res.* 1129, 34–42. <https://doi.org/10.1016/j.brainres.2006.10.063>.
 50. Otsuka, T., Thi Le, H., Kohsaka, A., Sato, F., Ihara, H., Nakao, T., and Maeda, M. (2020). Adverse effects of circadian disorganization on mood and molecular rhythms in the prefrontal cortex of mice. *Neuroscience* 432, 44–54. <https://doi.org/10.1016/j.neuroscience.2020.02.013>.
 51. Velakoulis, D., Walterfang, M., Mocellin, R., Pantelis, C., Dean, B., and McLean, C. (2009). Abnormal hippocampal distribution of TDP-43 in patients with-late onset psychosis. *Aust. N. Z. J. Psychiatr.* 43, 739–745. <https://doi.org/10.1080/00048670903001984>.
 52. Byrne, S., Heverin, M., Elamin, M., Bede, P., Lynch, C., Kenna, K., MacLaughlin, R., Walsh, C., Al Chalabi, A., and Hardiman, O. (2013). Aggregation of neurologic and neuropsychiatric disease in amyotrophic lateral sclerosis kindreds: A population-based case–control cohort study of familial and sporadic amyotrophic lateral sclerosis. *Ann. Neurol.* 74, 699–708. <https://doi.org/10.1002/ana.23969>.
 53. Turner, M.R., Goldacre, R., Talbot, K., and Goldacre, M.J. (2016). Psychiatric disorders prior to amyotrophic lateral sclerosis. *Ann. Neurol.* 80, 935–938. <https://doi.org/10.1002/ana.24801>.
 54. O'Brien, M., Burke, T., Heverin, M., Vajda, A., McLaughlin, R., Gibbons, J., Byrne, S., Pinto-Grau, M., Elamin, M., Pender, N., and Hardiman, O. (2017). Clustering of neuropsychiatric disease in first-degree and second-degree relatives of patients with amyotrophic lateral sclerosis. *JAMA Neurol.* 74, 1425–1430. <https://doi.org/10.1001/jamaneurol.2017.2699>.
 55. Rafferty, L.A., Cawkill, P.E., Stevelink, S.A.M., Greenberg, K., and Greenberg, N. (2018). Dementia, post-traumatic stress disorder and major depressive disorder: a review of the mental health risk factors for dementia in the military veteran population. *Psychol. Med.* 48, 1400–1409. <https://doi.org/10.1017/s0033291717001386>.
 56. Leonard, B.E. (2017). Major Depression as a Neuroprogressive Prelude to Dementia: What Is the Evidence? *Mod. Trends Pharmacopsychiatry* 31, 56–66. <https://doi.org/10.1159/000470807>.
 57. Kales, H.C., Gitlin, L.N., and Lyketsos, C.G. (2015). Assessment and management of behavioral and psychological symptoms of dementia. *Br. Med. J.* 350, h369. <https://doi.org/10.1136/bmj.h369>.
 58. Lawlor, B.A. (1996). Environmental and social aspects of behavioral disturbances in dementia. *Int. Psychogeriatr.* 8, 259–261. <https://doi.org/10.1017/s104161029700344x>.
 59. Roman Meller, M., Patel, S., Duarte, D., Kapczynski, F., and de Azevedo Cardoso, T. (2021). Bipolar disorder and frontotemporal dementia: A systematic review. *Acta Psychiatr. Scand.* 144, 433–447. <https://doi.org/10.1111/acps.13362>.

60. Mishima, K., Okawa, M., Hishikawa, Y., Hozumi, S., Hori, H., and Takahashi, K. (1994). Morning bright light therapy for sleep and behavior disorders in elderly patients with dementia. *Acta Psychiatr. Scand.* *89*, 1–7. <https://doi.org/10.1111/j.1600-0447.1994.tb01477.x>.
61. Van Someren, E.J., Kessler, A., Mirmiran, M., and Swaab, D.F. (1997). Indirect bright light improves circadian rest-activity rhythm disturbances in demented patients. *Biol. Psychiatr.* *41*, 955–963. [https://doi.org/10.1016/s0006-3223\(97\)89928-3](https://doi.org/10.1016/s0006-3223(97)89928-3).
62. Yoo, S.H., Yamazaki, S., Lowrey, P.L., Shimomura, K., Ko, C.H., Buhr, E.D., Slepka, S.M., Hong, H.K., Oh, W.J., Yoo, O.J., et al. (2004). PERIOD2::LUCIFERASE real-time reporting of circadian dynamics reveals persistent circadian oscillations in mouse peripheral tissues. *Proc. Natl. Acad. Sci. USA* *101*, 5339–5346. <https://doi.org/10.1073/pnas.0308709101>.
63. Tiscornia, G., Singer, O., and Verma, I.M. (2006). Production and purification of lentiviral vectors. *Nat. Protoc.* *1*, 241–245. <https://doi.org/10.1038/nprot.2006.37>.
64. Hughes, M.E., Hogenesch, J.B., and Kornacker, K. (2010). JTK_CYCLE: an efficient nonparametric algorithm for detecting rhythmic components in genome-scale data sets. *J. Biol. Rhythm.* *25*, 372–380. <https://doi.org/10.1177/0748730410379711>.
65. Umezu, T., Kuribara, H., and Tadokoro, S. (1989). Characteristics of circadian rhythm of wheel-running activity and drinking behavior in Mongolian gerbils. *Yakubutsu Seishin Kodo* *9*, 369–373.
66. Connolly, M.S., and Lynch, C.B. (1981). Circadian variation of strain differences in body temperature and activity in mice. *Physiol. Behav.* *27*, 1045–1049. [https://doi.org/10.1016/0031-9384\(81\)90368-1](https://doi.org/10.1016/0031-9384(81)90368-1).
67. Gordon, C.J. (1993). Twenty-four hour rhythms of selected ambient temperature in rat and hamster. *Physiol. Behav.* *53*, 257–263. [https://doi.org/10.1016/0031-9384\(93\)90202-q](https://doi.org/10.1016/0031-9384(93)90202-q).
68. Helwig, B.G., Ward, J.A., Blaha, M.D., and Leon, L.R. (2012). Effect of intraperitoneal radiotelemetry instrumentation on voluntary wheel running and surgical recovery in mice. *J. Am. Assoc. Lab. Anim. Sci.* *51*, 600–608.

STAR★METHODS

KEY RESOURCES TABLE

REAGENT or RESOURCE	SOURCE	IDENTIFIER
Antibodies		
Mouse anti-CLOCK	MBL International	Cat# D334-3
Rabbit anti-BMAL1	Abcam	Cat# 3350
Rabbit anti-PER2	Abcam	Cat# ab179813
Rabbit anti-TDP-43	Proteintech	Cat# 10782-2-AP
Rabbit anti-CRY1	Bethyl Laboratories	Cat# A302-614A-T
Rabbit anti-CRY2	Bethyl Laboratories	Cat# A302-615A
Mouse anti-GAPDH	Proteintech	Cat# 60004
Mouse anti-β actin	Proteintech	Cat# 66009
Anti-rabbit HRP-linked secondary	Cell Signaling	Cat# 7074
Anti-mouse HRP-linked secondary	Cell Signaling	Cat# 7076
Rabbit anti-cFos	Cell Signaling	Cat# 2250
Goat anti-mouse, Alexa-Fluor-488	Thermo Fisher Scientific	Cat# A11001
Gonkey anti-rabbit, cyanine Cy3	Jackson ImmunoResearch	Cat# 711-165-152
Deposited data		
The original data generated in this work has been deposited in Mendeley Data	This work	Mendeley Data: https://doi.org/10.17632/dnnyj8ftk.1
Bacterial and virus strains		
Virus: pAAV-U6-shRNA(<i>Tdp-43</i>)-CMV-EGFP-WPRE (Serotype: AAV2/9)	Shanghai OBiO Technology	Cat# Y25761
Virus: pAAV-U6-shRNA(CON)-CMV-EGFP-WPRE (Serotype: AAV2/9)	Shanghai OBiO Technology	Cat# Y11982
Bacterial strain: Trans1-T1 Phage Resistant	TransGen	Cat# CD501-02
Chemicals, peptides, and recombinant proteins		
PMSF	AMRESCO	Cat# 0754
Protease inhibitors, Complete Mini, EDTA-free	Roche	Cat# 11836170001
B27	Thermo Fisher	Cat# 17504044
Critical commercial assays		
Bright- Glo™ Luciferase Assay System	Promega	Cat# E2620
Phanta Super-Fidelity DNA Polymerase	Vazyme	Cat# P501-d1
Lipofectamine 2000	Thermo Fisher	Cat# 12566014
Lipofectamine 3000	Thermo Fisher	Cat# L3000015
PrimeScript™ RT Master Mix	Takara	Cat# RR036A
SsoAdvanced™ Universal SYBR® Green Supermix	BioRad	Cat# 1725275
M5 SuperFast Seamless Cloning Mix	Mei5Bio	Cat# MF017
Experimental models: Cell lines		
HEK-293T cells	ATCC	RRID: CVCL_0063
U2OS cells	ATCC	RRID: HTB-96
Experimental models: Organisms/strains		
Mouse: C57BL/6J	The Jackson Laboratory	JAX Stock#: 000664
Mouse: mPer2 ^{Luc} ; B6.129S6-Per2 ^{tm1Jt} /J	Yoo et al. ⁶²	JAX Stock#: 006852

(Continued on next page)

Continued

REAGENT or RESOURCE	SOURCE	IDENTIFIER
Oligonucleotides		
Primers for qPCR detection, see Tables S2 and S3	This paper	N/A
shRNA for TDP-43 knock down, see Table S1	This paper	N/A
Primers for cDNA amplification, see Table S5	This paper	N/A
Recombinant DNA		
Plasmid: pGL3-SV40-Ebox-dLuc	This paper	N/A
Plasmid: pcDNA3.1-CMV-3F6H-human <i>Clock</i>	This paper	N/A
Plasmid: pcDNA3.1-CMV-3F6H- human <i>Bmal1</i>	This paper	N/A
Plasmid: pcDNA3.1-CMV-3F6H- human <i>Cry1</i>	This paper	N/A
Plasmid: pcDNA3.1-CMV-3F6H-human <i>Tdp43</i>	This paper	N/A
Plasmid: pcDNA3.1-CMV-3F6H-EGFP	This paper	N/A
Plasmid: pCDH-CMV-human <i>Tdp43</i> -EF1a-GFP	This paper	N/A
Plasmid: pREV	Tiscornia et al. ⁶³	N/A
Plasmid: pVSVG	Tiscornia et al. ⁶³	N/A
Plasmid: pMDL	Tiscornia et al. ⁶³	N/A
Plasmid: pLKO.1-U6-shTDP-43	This paper	N/A
Plasmid: pLKO.1-control	This paper	N/A
Software and algorithms		
LumiCycle analysis	Actimetrics	N/A
JTK Cycle	Hughes et al. ⁶⁴	https://openwetware.org/mediawiki/index.php?title=HughesLab:JTK_Cycle&oldid=971822
BioDare2	Zielinski et al. ²³	https://biodare2.ed.ac.uk
Clock lab software	Actimetrics	N/A
PRISM	GraphPad	https://www.graphpad.com/scientific-software/prism/
Microsoft Excel	Microsoft	N/A
rowheadOther		
SDS-PAGE loading buffer (6X)	Beyotime	Cat# P0015F
Thermo Scientific Pierce IP Lysis Buffer	Thermo Fisher Scientific	Cat# 87788
TRlzol™ Reagent	Thermo Fisher	Cat# 15596018
DAPI	Sigma-Aldrich	Cat# D9542
DMEM	Gibco	Cat# 11965092
Opti-MEM® I Reduced-Serum Medium (1X), liquid	Invitrogen	Cat# 51985034
Archimed X6 qPCR machine	RocGene Tecnology Co.	N/A

RESOURCE AVAILABILITY

Lead contact

Further information and requests for resources and reagents should be directed to and will be fulfilled by the lead contact, Eric Erquan Zhang (zhangerquan@nibs.ac.cn).

Materials availability

All unique reagents generated in this study are available from the [lead contact](#) upon request.

Data and code availability

- Original data have been deposited at Mendeley Data (<https://data.mendeley.com/>) and are publicly available as of the date of publication. Accession number is listed in the [key resources table](#).

- This paper does not report original code.
- Any additional information required to reanalyze the data reported in this paper is available from the [lead contact](#) upon request.

EXPERIMENTAL MODEL AND STUDY PARTICIPANT DETAILS

Animal procedures

All animal procedures were conducted in accordance with the guidelines of the Institutional Animal Care and Use Committees (IACUC) at the National Institute of Biological Sciences (NIBS). Male and female C57BL/6J mice aged between 8-12 weeks were used for this study. The mice were maintained under natural light-dark cycle (12 hours of light and 12 hours of darkness), with *ad libitum* access to food and water. Room temperature was maintained between 18°C and 22°C, with humidity ranging from 40 to 70%. Random selection of mice was carried out for both virus injection and behavioral tests.

METHOD DETAILS

Cell culture

Human bone osteosarcoma epithelial (U2OS) (ATCC: RRID: HTB-96) cells and HEK293T (ATCC: CVCL_0063) cells were cultured at 37°C in a 5% CO₂ atmosphere. Cells were cultured in Dulbecco's Modified Eagle's Medium (DMEM, Thermo Fisher) supplemented with 10% fetal bovine serum (FBS, Gibco) and 100 U/ml Penicillin-Streptomycin (PS, Thermo Fisher).

Plasmids construction and stable cell line generation

The TDP-43 sequence was amplified from human cDNA using the primers listed in [Table S5](#) and cloned into pCDNA3.1(+) and Lenti-vector (PCDH-CMV) using the seamless cloning method. The sequences of shRNA-TDP-43 ([Table S1](#)) were synthesized and cloned into pLKO.1-U6-vector (referred to as shTDP-43 in the text). Stable shTDP-43 and shCON cell lines were generated as previously described.⁶³ Briefly, HEK293T cells were transfected with PCDH-CMV-TDP-43 or pLKO-U6-shTDP-43/shCON and lentiviral packaging plasmids using Lipofectamine 3000 (Thermo Fisher) following the manufacturer's instructions. 4 µg of total DNA plasmid, 8 µl of Lipofectamine 3000 and 500 µl of opti-MEM were mixed and added to each well of 6 well-plate (according the mass ratio pMDL:pVSVG:pREV = 270:176:95, 2.23 µg of packaging plasmids mixture and 1.77 µg PCDH-CMV-TDP-43 or pLKO-U6-shTDP-43 / shcon). After transfection for 48 hours, the lentivirus-containing cell supernatant was filtered through a 0.45 µm filter and used to infect the target cell lines. Infected cells were sorted with flow cytometry, and knock-down efficiency of shTDP-43 was assessed via qPCR (for primers, see [Table S2](#)).

Luciferase assay

In the luciferase assay, HEK293T cells were transfected with 20 ng Ebox-dLuc reporter and varying amounts of other plasmids (30, 50 or 80 ng pcDNA3.1-TDP-43, 160, 130 or 100 ng mixture of pcDNA3.1-Clock and pcDNA3.1-Bmal1, 10 ng pcDNA3.1-Cry1, and appropriate pcDNA3.1-EGFP to reach a total of 200 ng) in 96-well plates. This assay was performed 48 hours post-transfection using the Promega Dual-Luciferase Reporter Assay System according to the manufacturer's instructions. All experiments were conducted at least three times.

Quantitative real-time PCR (qRT-PCR) analysis

Total RNA was extracted from cells using TRIzol (Thermo Fisher). cDNA was synthesized using a PrimeScript RT Master Mix Real-time RT-PCR Kit (Takara) and analyzed by qRT-PCR with a SYBR Green Supermix kit (Bio-rad). For the time course qPCR, cells were synchronized using a 50% serum shock for two hours, followed by harvesting at six time points over 24 hours. Gene primers for qPCR are listed in [Table S3](#), and rhythmicity was analyzed using JTK_Cycle.⁶⁴

Western blotting

For cell extracts, U2OS cells were lysed in SDS sample buffer and boiled. For tissue extracts, brains were homogenized and lysed in RIPA buffer. Protein samples were separated by SDS-PAGE, transferred to polyvinylidene difluoride membranes (Millipore), the membranes were incubated in 5% milk at room temperature for 1 hour, followed by overnight incubation with primary antibodies at 4°C, the membranes with combined primary antibodies then visualized using horseradish peroxidase-conjugated secondary antibodies for 1 h at room temperature. The blot signal was detected using Immobilon ECL substrate (Millipore). Primary antibodies included anti-CLOCK (MBL, 1:2000), anti-BMAL1 (Abcam, 1:1000), anti-PER2 (Abcam, 1:2000), anti-CRY1 (Bethyl Laboratories, 1:1000), anti-CRY2 (Bethyl Laboratories, 1:1000), anti-TDP-43 (Proteintech, 1:2000), anti-GAPDH (Proteintech, 1:5000) and anti-β-actin (Proteintech, 1:10000). Secondary antibodies were anti-mouse IgG-HRP and anti-rabbit IgG-HRP (CST). The time-course of protein level was analyzed with JTK_Cycle software package.⁶⁴

Immunofluorescent staining

For brain tissue staining, mice were perfused with cold 4% PFA (4% PFA in 0.01 M PBS, pH 7.4), the brain was dissected and immersed in 4% PFA for 4~6 h at room temperature, followed by cryoprotection in 30% sucrose overnight until it sank to the bottom of the tube. Subsequently, the brain was frozen on dry ice and embedded in OCT. Coronal brain slices, 40 µm thickness, were sectioned using a cryostat at -20°C. For TDP-43 staining in SCN, the SCN region was collected from each slice (bregma -0.22 mm to -0.82 mm); for TDP-43 staining in hippocampus,

the hippocampal region was collected from every third brain slice (bregma -0.94 mm to -1.94 mm); for c-Fos staining in PFC (bregma 1.98 mm to 0.74 mm), NAC (bregma 1.94 mm to 0.62 mm), amygdala (bregma -0.58 mm to -2.3 mm), and hippocampus (bregma -0.94 mm to -1.94 mm), each of these regions was collected from every third brain slice and 4-8 slices were selected after staining for statistical analysis. These brain slices were washed three times with 0.3% PBST (0.3% Triton X-100 in PBS) and blocked with 0.2% Bovine Serum Albumin (BSA) for 2 h at room temperature. Following blocking, the slices were incubated with primary antibodies overnight at 4°C and then with corresponding fluorescence-conjugated secondary antibodies for 2 hours in darkness at room temperature. Primary antibodies included rabbit polyclonal anti-c-Fos (CST, 1:1000), and rabbit polyclonal anti-TDP-43 (Proteintech, 1:100). Fluorescence-conjugated secondary antibodies included Alexa-Fluor-488 goat anti-mouse IgG (Thermo Fisher Scientific, 1:1000), cyanine Cy3 donkey anti-rabbit IgG (Jackson ImmunoResearch, 1:1000), and Alexa-Fluor-647 donkey anti-rabbit IgG (Jackson ImmunoResearch, 1:1000). Brain slices were stained with DAPI and imaged using an Olympus SLIDEVIEW VS200 digital slide scanner.

Stereotactic virus injection

Adult C57BL/6J and *mPer2-Luc* knockin (aged 8–10 weeks old) mice were euthanized with pentobarbital sodium and placed in a stereotaxic rig, then injected with AAV9-U6-shRNA (TDP-43 or CON)-CMV-EGFP-WPRE (referred to as AAV-shTDP-43 or AAV-shCON) into the bilateral SCN or CA1 of the hippocampus using stereotactic coordinates (ML: ± 0.25 mm, AP: -0.42 mm, DV: 5.42 mm for SCN, ML: ± 1.68 mm, AP: -2 mm, DV: 1.87 mm for CA1 of the hippocampus). The injection was conducted using a glass cannula and a microsyringe pump at a specific flow rate into each SCN or CA1 region for 400 nl unilaterally. The glass cannula was left in place for 20 mins before withdrawal. The titre of AAV-shTDP-43 and AAV-shCON was higher than 2×10^{12} vg/ml.

Bioluminescence rhythms in cell and tissue culture

To record rhythmicity in shTDP-43 knockdown cells and SCN explants, human U2OS cells harboring *PER2-LUC* infected with shcon and shTDP-43 lentivirus were cultured in 3.5 cm dishes, after growing to 95% confluence, followed by replacing with XM medium (DMEM medium containing 10 mM HEPES pH 7.0, 0.1 mM D-luciferin, 50 U/ml penicillin-streptomycin and 2% B27 supplement) and sealed with high vacuum grease. Finally, the cells were subjected to Lumicycle recording for 5–7 days. For recording the bioluminescence rhythmicity of SCN, the adult *mPer2-Luc* knockin male mice were injected with AAV-shTDP-43 or AAV-shCON, after expressing for 3 weeks, mice were euthanized and harvested quickly in cold HBSS buffer, coronally sliced the brain with 250 μm on a vibrating microtome until the visible SCN appeared, the SCN tissues were cultured on Millicell culture membrane (Millipore) in 3.5 cm dishes and recording for 7–9 days. Data were analyzed using the LumiCycle Analysis software.

Wheel-running analysis

Voluntary wheel running is widely used in circadian rhythm studies. Male mice were placed in cages with a cart-shaped wheel to allow voluntary movement of the mice on the wheel, the spins are transferred electronically to a USB hub so that the frequency and rate of runs can be captured via a software program for data storage and analysis over different time periods.⁶⁵ Three weeks after AAV-shCON and AAV-shTDP-43 expression in SCN or hippocampus, mice were individually housed in cages equipped with infrared sensors to detect wheel-running activity. After ZT12 (lights out) on day 14 of entrainment under LD cycle, mice were switched to DD phase to analyze their endogenous circadian rhythms with the ClockLab system, the locomotor activity and period were calculated using standard parameters in the ClockLab software.

Core body temperature recording

The E-mitter system is capable of collecting animal core body temperature and general activity data. Circadian rhythms of core body temperature exhibit maximum temperatures during dark phase and minimum temperatures during light phase.^{66,67} After three weeks of AAV-shCON and AAV-shTDP-43 expression in SCN of male and female mice, mice were anesthetized with pentobarbital sodium and placed in a supine position. The abdomen of each mouse was then shaved with a shaving device and disinfected with 75% alcohol, before introducing an approximately 1 cm incision through the skin and abdominal muscle layers by sterile technique. Each E-mitter (Starr Life Sciences) required at least 5 hours of sterilization before use and repeated flushing in 0.9% sterile saline solution before placement into the peritoneal cavity. The E-mitter was sutured to the peritoneal wall using a single-needle non-absorbable suture, and then the peritoneal muscle layer and skin layer were sutured separately with absorbable sutures.⁶⁸ After surgery, each mouse was placed in a clean cage with food and water *ad libitum* and allowed 1 week to recover. After this recovery/acclimation period, mice were treated with LD cycle for 3 days, followed by three days of DD condition. The rhythmicity was analyzed with BioDare2 software package, including period, amplitude.²³

Behavioral analyses

Behavioral tests were conducted at least 3 weeks after stereotactic virus injection in male and female mice. Except for sucrose preference tests that were conducted from ZT0 – ZT12 (8:00 am – 8:00 pm) or ZT12 – ZT24 (8:00 pm – 8:00 am), all other behavioral assays were performed during the light phase (ZT4 – ZT8, i.e. 12:00 am–4:00 pm). Except for the sucrose preference test, mice were transferred to test room to adaptation for 1 hour. The behavioral tests were conducted in the following order: Sucrose Preference Test, Open Field Test, Forced Swimming Test, and Tail Suspension Test, with a 2-day interval between two individual behavioral assays, and behavioral equipment were cleaned with 75% ethanol between each batch of mice.

Open Field Test (OPT): Used to examine anxiety-like behavior. Mouse activity was monitored in an open field apparatus (44 cm × 44 cm × 30 cm), the track of mice was monitored by video camera (SARGO) and allowed to record for 5 mins, and total distance traveled, percentage of time spent in open field, percentage of distance traveled in open field were analyzed using Smart v3.0.

Sucrose Preference Test (SPT): Performed to evaluate rewarding activities and anhedonia. Mice were provided with two bottles, one containing 2% sucrose and the other pure water. Prior to the test, mice were adapted to the two drinking bottles in their home cages for two days, the positions of the two bottles are swapped daily to reduce any biased side effects. Following this acclimation, mice freely choose to consume sugar water or pure water, and sucrose preference was calculated following this formula: sucrose intake percentage% = sucrose intake / (sucrose + water intake) *100%.

Forced Swimming Test (FST): A behavioral despair-based test where mice were placed in a transparent beaker (10 cm diameter) containing water (22°C~26°C) at a depth of 20 cm and monitored for 6 mins by video camera. The duration of immobility was analyzed the 4 mins of recording following by 2 mins of habituation. The water was changed and the transparent beaker was cleaned for each mouse tested. The mice were considered immobile only when they floating in water and were completely motionless.

Tail Suspension Test (TST): For this despair-based behavioral test, mice were suspended by their tails at a height of 40 cm from the ground and monitored for 6 mins by video camera. The duration of immobility was scored during the last 4 min of recording following by 2 min of habituation. The mice were considered immobile only when they hung upside down completely motionless.

QUANTIFICATION AND STATISTICAL ANALYSIS

Statistical analysis was performed using Excel and GraphPad Prism 8 software. It included one-way and two-way analysis of variances (ANOVA) followed by Tukey's multiple comparisons test and Sidak's multiple comparisons, as well as unpaired two-tailed for two group comparisons. All statistical analysis for individual experiments are described in indicated figure legends. Error bars represent the standard error of the mean \pm SEM, *p < 0.05, **p < 0.01, ***p < 0.001, ****p < 0.0001. The detailed results of each statistical analysis are provided in [Table S6](#).